showed that the hemoglobin level and platelet count were decreased to 6.4 g/dL and 82,000/μL, respectively. An abdominal computed tomography (CT) scan showed hepatomegaly with a heterogeneous low density area expanding from the medial segment to the right lobe of the liver, and the leakage of contrast material into parenchyma during the arterial phase, suggesting the diagnosis of liver hemorrhage (Fig. 2a). There was little intraperitoneal bleeding. With rapid transfusion of red cells, a hepatic angiogram was performed via the common hepatic artery. Because active bleeding was observed within liver parenchyma (Fig. 2b), obstructing material (Gelpart® Molecular Devices, Nippon Kayaku Co. Ltd., Tokyo, Japan) was injected into the anterior and posterior branches of the hepatic artery to control active bleeding. Despite these treatments, hemoglobin levels gradually decreased from 11.1 to 3.8 g/dL 8 h after the obstruction therapy. The abdomen was further distended and pitting edema appeared in the lower body. Repeated abdominal CT showed massive intraperitoneal bleeding compared with that of the previous day, and a narrowed inferior vena cava caused by hepatic enlargement was detected. He died 4 days after the onset of acute hepatic hemorrhage. The autopsy indicated

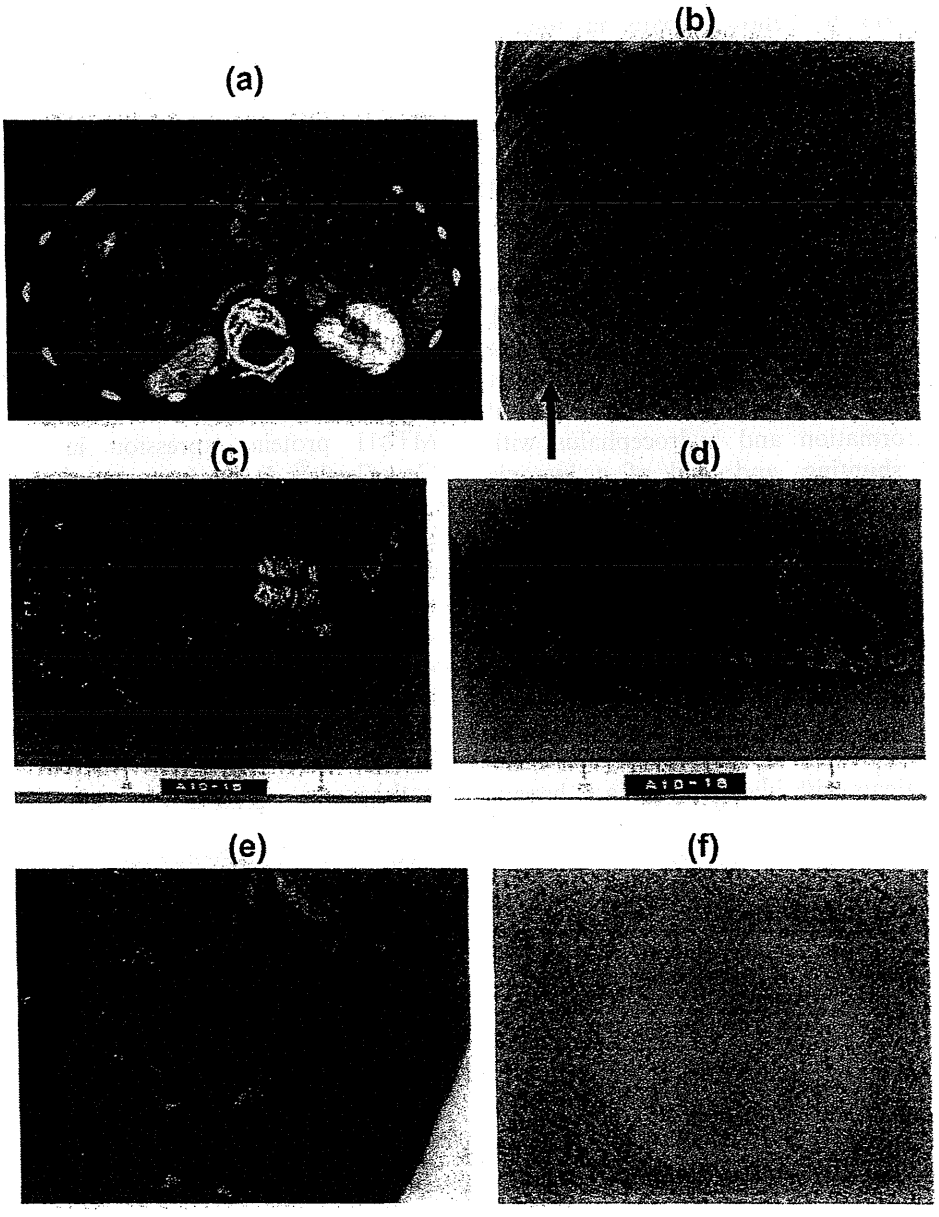

Fig. 2. Radiological and pathological findings of periosis hepatis. (a) Contrast abdominal CT shows hepatomegaly and a heterogeneous low density area extending from the medial segment to the right lobe of the liver. Contrast dye had leaked into the parenchyma (arrow) during the arterial phase. (b) A hepatic angiogram shows a number of retained contrast agents and some active bleeding (arrow) within liver parenchyma. (c and d) Autopsy findings show expansive intraperitoneal bleeding caused by rupture at the right hepatic capsule, and multiple variable-sized cystic blood-filled spaces were found in a section of the liver. (e) Multiple blood-filled spaces within the liver parenchyma can be seen (H & E). (f) Immunohistochemically, the inner surface of the blood-filled space is devoid of CD31-positive endothelial lining in contrast to the sinusoidal endothelia.

expansive intraperitoneal bleeding caused by rupture of the right hepatic capsule (Fig. 2c). Multiple variable-sized cystic blood-filled spaces and hemorrhagic necrosis were found in the liver (Fig. 2d). Histopathologically, the liver contained multiple blood-filled spaces (Fig. 2e) that were devoid of CD31-positive endothelial lining (Fig. 2f), which was compatible with peliosis hepatis.

3. Discussion

Peliosis hepatis is a rare fatal disorder with a number of causes, and is defined as multiple, variable-sized, cystic, blood-filled spaces through the liver parenchyma, in which spaces are not covered by endothelium of blood vessels histopathologically [9]. Peliosis hepatis has mostly been reported in adult patients associated with chronic wasting disorder [10], human immunodeficiency virus infection [11–12], oral contraceptives [13], androgenic steroids [14], and *Bartonella henselae* infection [15], and is idiopathic [16]. In children, peliosis hepatis is rare and has only been reported with androgenic steroids [17–18], *Escherichia coli* pyelonephritis [19], and XLMTM [4–7].

In XLMTM, only six children with peliosis hepatis, including our case, have been reported (Table 1) [4–7], and five of them developed acute onset multiple organ failure. The remaining child was detected by chance at the time of the autopsy, and this child had a central nervous system malformation and hydrocephalus with ventriculo-peritoneal shunting, and died of a hypoxic episode at 4 years old. The mean age at onset of peliosis hepatis was 4 years. Antecedent infection before hepatic hemorrhage was observed in three patients, including our patient. An elevated liver function test was observed in three patients, including our patient, but was normal in two. Five of six patients died of acute fatal hepatic hemorrhage. One patient survived after laparotomy and transarterial embolization [5]. Therefore, peliosis hepatis with XLMTM is characterized by difficult-to-treat acute onset. Some adult patients with idiopathic peliosis hepatis have received successful emergent hepatectomy, liver transplantation, and arterial embolization [16,20]. However, once hepatic hemorrhage from peliosis hepatis occurs, it is usually difficult to control bleeding, as observed in our patient. Therefore, reducing the incidence and prompt recognition of hepatic hemorrhage are mandatory for XLMTM patients.

The diagnosis of peliosis hepatis is difficult and often missed or delayed because of the atypical findings on standard radiological tests. A previous report indicated that ultrasonic examination is useful to detect abnormal findings according to various liver conditions, and can show perinodular and intranodular vascularity in patients with peliosis hepatis [21]. Other imaging systems, including CT, magnetic resonance imaging, and angiography can also be helpful for diagnosis of peliosis hepatis [18,21]. Our patient showed persistent mild elevations in a serum liver function test before the episode of acute hemorrhage. He had not received a routine ultrasonic examination, and CT findings on admission indicated no hepatic lesion, suggesting hemorrhage or peliosis hepatis. Therefore, fatal hepatic hemorrhage from peliosis hepatis was induced by an unknown cause after admission.

The mechanism of peliosis hepatis remains to be fully elucidated. And the causal relationship between peliosis hepatis and XLMTM is poorly understood, although MTM1 protein expression in liver are reported in GeneCards®. It has been reported that a mechanical in-exsufflator (MI-E) is safe and effective for respiratory infections of pediatric patients with neuromuscular disorders [22]. MI-E was initially used for removing secretions in our case, and fatal hepatic hemorrhage occurred on the next day of MI-E adoption. In some reports describing the mechanism of peliosis hepatis, blockade of liver blood outflow and increased sinusoidal pressure in patients with abnormality of the sinusoidal barrier were important factors contributing to the pathogenesis [23,24]. In our case, there were no

Table 1
Summary of peliosis hepatis in XLMTM patients.

No.	Age	Severity of XLMTM	Cognitive development	Detection of PH	Known liver dysfunction	Infection at the onset of PH	Diagnosis	Status
1[4]	5 y	Severe	Normal	Hepatic hemorrhage	Yes	Un-documented	Autospy	Deceased
2[4]	4 y	Severe	Normal	By chance (autospy)	No	Un-documented	Autospy	Deceased
3[5]	3 y	Severe/ moderate	Normal	Hepatic hemorrhage	No	URI otitis media	CT	Improved
4[6]	2 y 6 m	Severe	Un-documented	Hepatic hemorrhage	(Un-documented)	Un-documented	Autospy	Deceased
5[7]	5 y	Severe	Un-documented	Hepatic hemorrhage	Yes	Fever	Autospy	Deceased
6 (present patient)	5 y	Severe	Slightly retarded	Hepatic hemorrhage	Yes	Pneumonia	Autospy	Deceased

PH: peliosis hepatis, URI: upper respiratory infection, CT: computed tomography.

manifestations of a blockade of liver blood outflow, but the elevation in inferior vena cava pressure caused by a sharp rise in intrapleural pressure using MI-E might have been a potential cause of peliosis hepatis.

In conclusion, peliosis hepatis is a rare but important fatal complication that may occur more often once genetic or other therapies for XLMTM become available with a resulting increase in life expectancy. To avoid fatal hepatic hemorrhage from peliosis hepatis, routine liver function tests and abdominal imaging studies are recommended for all XLMTM patients. In addition, it might be necessary to carefully check liver imaging tests, especially at the time of using mechanical ventilation.

References

[1] Spiro AJ, Shy GM, Gonatas NK. Myotubular myopathy. Persistence of fetal muscle in an adolescent boy. Arch Neurol 1966;14:1–14.

[2] Romero NR. Centronuclear myopathies: a widening concept. Neuromuscul Disord 2010;20:223–8.

[3] Laporte J, Biancalana V, Tanner SM, et al. MTM1 mutation in X-linked myotubular myopathy. Hum Mutat 2000;15:393–409.

[4] Herman GE, Finegold M, Zhao W, Gouyon B, Metzenberg A. Medical complications in long-term survivors with X-linked myotubular myopathy. J Pediatr 1999;134:206–14.

[5] Wang SY, Ruggles S, Vade A, Newman BM, Borge MA. Hepatic rupture by peliosis hepatis. J Pediatr Surg 2001;36:1456–9.

[6] Karger B, Varchmin-Schultheib K, Fechner G. Fatal hepatic haemorrhage in a child-peliosis hepatis versus maltreatment. Int J Legal Med 2005;119:44–6.

[7] Yano T, Toyono M, Watanabe Y, Sawaishi Y. A 5-year old boy of X-linked myotubular myopathy died of hepatic rapture from peliosis hepatis (in Japanese). No To Hattatsu 2010;42:S348.

[8] Tsai TC, Horinouchi H, Noguchi S, et al. Characterization of *MTM1* mutations in 31 Japanese families with myotubular myopathy, including a patient carrying 240 kb deletion in Xq28 without male hypogenitalism. Neuromuscul Disord 2005;15:245–52.

[9] Zak FG. Peliosis hepatis. Am J Pathol 1950;26:1–15.

[10] Simon DM, Krause R, Galambos JT. Peliosis hepatis in a patient with marasmus. Gastroenterology 1988;95:805–9.

[11] Perkocha LA, Geaghan SM, Yen B, et al. Clinical and pathological features of bacillary peliosis hepatis in association with human immunodeficiency virus infection. N Engl J Med 1990;323:1581–6.

[12] Scoazec J-Y, Marche C, Girard P-M, et al. Peliosis hepatis and sinusoidal dilatation during infection by human immunodeficiency virus (HIV). Am J Pathol 1988;131:38–47.

[13] Testa G, Panaro F, Sankary H, et al. Peliosis hepatis in a living related liver transplantation donor candidate. J Gastroenterol Hepatol 2006;21:1075–7.

[14] Bagheri SA, Boyer JL. Peliosis hepatis associated with androgenic–anabolic steroid therapy. A severe form of hepatic injury. Ann Intern Med 1974;81:610–8.

[15] Koehler JE, Sanchez MA, Garrido CS, et al. Molecular epidemiology of bartonella infections in patients with bacillary angiomatosis–peliosis. N Engl J Med 1997;337:1876–83.

[16] Hyodo M, Mogensen AM, Larsen PN, et al. Idiopathic extensive peliosis hepatis treated with liver transplantation. Hepatobiliary Pancreat Surg 2004;11:371–4.

[17] Tsirigotis P, Sella T, Shapira MY, et al. Peliosis hepatis following treatment with androgen-steroids in patients with bone marrow failure syndromes. Haematologica 2007;92:e106–10.

[18] Battal B, Kocaoglu M, Atay AA, Bulakbasi N. Multifocal peliosis hepatis: MR and diffusion-weighted MR-imaging findings of an atypical case. Ups J Med Sci 2010;115:153–6.

[19] Jacquemin E, Pariente D, Fabre M, Huault G, Valayer J, Bernard O. Peliosis hepatis with initial presentation as acute hepatic failure and intraperitoneal hemorrhage in children. J Hepatol 1999;30:1146–50.

[20] Hayward SR, Lucas CE, Ledgerwood AM. Recurrent spontaneous intrahepatic hemorrhage from peliosis hepatis. Arch Surg 1991;126:782–3.

[21] Iannaccone R, Federle MP, Brancatelli G, et al. Peliosis hepatis: spectrum of imaging findings. Am J Roentgenol 2006;187:W43–52.

[22] Miske LJ, Hickey EM, Kolb SM, Weiner DJ, Panitch HB. Use of the mechanical in-exsufflator in pediatric patients with neuromuscular disease and impaired cough. Chest 2004;125:1406–12.

[23] Degott C, Rueff B, Kreis H, Duboust A, Potet F, Benhamou JP. Peliosis hepatis in recipients of renal transplants. Gut 1978;19:748–53.

[24] Zafrani ES, Cazier A, Baudelot AM, Feldmann G. Ultrastructural lesions of the liver in human peliosis. A report of 12 cases. Am J Pathol 1984;114:349–59.

Available online at www.sciencedirect.com

SciVerse ScienceDirect

Neuromuscular Disorders 23 (2013) 675–681

www.elsevier.com/locate/nmd

Limb-girdle muscular dystrophy type 2I is not rare in Taiwan

Wen-Chen Liang[a,b], Yukiko K. Hayashi[c,d], Megumu Ogawa[c], Chien-Hua Wang[a], Wan-Ting Huang[e], Ichizo Nishino[c,d], Yuh-Jyh Jong[a,f,g,h,*]

[a] *Department of Pediatrics, Kaohsiung Medical University Hospital, Kaohsiung Medical University, Kaohsiung, Taiwan*
[b] *Department of Pediatrics, School of Medicine, College of Medicine, Kaohsiung Medical University, Kaohsiung, Taiwan*
[c] *Department of Neuromuscular Research, National Institute of Neuroscience, National Center of Neurology and Psychiatry, Tokyo, Japan*
[d] *Department of Clinical Development, Translational Medical Center, National Center of Neurology and Psychiatry, Tokyo, Japan*
[e] *Department of Pathology, Kaohsiung Medical University Hospital, Kaohsiung Medical University, Kaohsiung, Taiwan*
[f] *Department of Laboratory Medicine, Kaohsiung Medical University Hospital, Kaohsiung Medical University, Kaohsiung, Taiwan*
[g] *Graduate Institute of Medicine, College of Medicine, Kaohsiung Medical University, Kaohsiung, Taiwan*
[h] *Department of Biological Science and Technology, College of Biological Science and Technology, National Chiao Tung University, Hsin-Chu, Taiwan*

Received 9 March 2013; received in revised form 15 May 2013; accepted 24 May 2013

Abstract

Alpha-dystroglycanopathy is caused by the glycosylation defects of α-dystroglycan (α-DG). The clinical spectrum ranges from severe congenital muscular dystrophy (CMD) to later-onset limb girdle muscular dystrophy (LGMD). Among all α-dystroglycanopathies, LGMD type 2I caused by *FKRP* mutations is most commonly seen in Europe but appears to be rare in Asia. We screened uncategorized 40 LGMD and 10 CMD patients by immunohistochemistry for α-DG and found 7 with reduced α-DG immunostaining. Immunoblotting with laminin overlay assay confirmed the impaired glycosylation of α-DG. Among them, five LGMD patients harbored *FKRP* mutations leading to the diagnosis of LGMD2I. One common mutation, c.948delC, was identified and cardiomyopathy was found to be very common in our cohort. Muscle images showed severe involvement of gluteal muscles and posterior compartment at both thigh and calf levels, which is helpful for the differential diagnosis. Due to the higher frequency of LGMD2I with cardiomyopathy in our series, the early introduction of mutation analysis of *FKRP* in undiagnosed Taiwanese LGMD patients is highly recommended.

Keywords: Alpha-dystroglycan; Alpha-dystroglycanopathy; Limb-girdle muscular dystrophy type 2I; *FKRP*; Dilated cardiomyopathy; Glycosylation defect; Laminin binding; Muscle imaging

1. Introduction

Alpha-dystroglycanopathy is a group of muscular dystrophies caused by altered glycosylation of α-dystroglycan (α-DG), which is one of the components of dystrophin–glycoprotein complex [1,2]. The clinical phenotypes form a broad spectrum, ranging from severe congenital muscular dystrophy (CMD) with or without ocular and central nervous system involvement to later-onset limb girdle muscular dystrophy (LGMD) [3–5].

A number of genes have been reported to cause α-dystroglycanopathy, including *POMT1*, *POMT2*, *POMGnT1*, *FKTN*, *FKRP*, and *LARGE* that are known to be involved in glycosylation of α-DG, and *DAG1*, which encodes DG itself [6–11]. Recently, the number of genes associated with α-dystroglycanopathy has been increasing to include *ISPD*, *TMEM5*, *GTDC2*, *B3GNT1*, *DOLK*, *DPM2* and *DPM3* [12–19]. Patients with all

* Corresponding author. Address: Department of Pediatrics, Kaohsiung Medical University Hospital, Kaohsiung Medical University, No. 100, Tz-You 1st Rd., Kaohsiung 80708, Taiwan. Tel.: +886 7 312 1101x6507; fax: +886 7 321 2062.
E-mail addresses: yjjong@kmu.edu.tw, yjjong@gap.kmu.edu.tw (Y.-J. Jong).

0960-8966/$ - see front matter © 2013 Published by Elsevier B.V.
http://dx.doi.org/10.1016/j.nmd.2013.05.010

kinds of α-dystroglycanopathy are inherited with autosomal recessive trait.

Among those causative genes for α-dystroglycanopathy, *FKRP* mutations are the most frequently seen in the Caucasian population, causing LGMD2I and congenital muscular dystrophy type 1C (MDC1C). In the Asian population, on the other hand, the most common α-dystroglycanopathy is Fukuyama congenital muscular dystrophy and LGMD2M caused by the mutations in *FKTN* [20–24]. This phenomenon may be caused by the founder effect of c.826C>A substitution in *FKRP* and the ancestral insertion of a SINE-VNTR-Alu (SVA) retrotransposon in *FKTN* in different geographic areas [21,25]. Recently, an increasing number of patients having *FKTN* mutations were identified outside Asia but so far few Asian patients with LGMD2I caused by *FKRP* mutations have been reported [26–29].

In this study, we found that LGMD2I is common in the Taiwanese patients with α-dystroglycanopathy due to a common mutation, c.948delC (p.Cys317Alafs*111), which may cause more severe phenotype and cardiomyopathy.

2. Materials and methods

2.1. Patients

Forty patients clinically and pathologically diagnosed as LGMD and 10 patients with CMD who received muscle biopsy in Kaohsiung Medical University Hospital from January, 2008 to December, 2011 were enrolled. LGMD was defined as progressive proximal-dominant muscle weakness with characteristic dystrophic changes in muscle pathology. CMD was recognized as infantile floppiness with dystrophic muscle. Patients with deficiencies of dystrophin, sarcoglycans, dysferlin, merosin or collagen VI were excluded by immunohistochemistry beforehand. All merosin deficiency patients were confirmed to have *LAMA2* mutations [30]. This study was approved by the institutional review board of the Kaohsiung Medical University Hospital.

2.2. Histochemistry

Biopsied muscle specimens were frozen in isopentane cooled in liquid nitrogen. A serial frozen section was stained by a battery of histochemical methods including hematoxylin and eosin (H&E), modified Gomori-trichrome (mGt) and NADH-tetrazolium reductase (NADH-TR).

2.3. Immunohistochemistry

Frozen sections of 6 μm thickness were used for immunohistochemistry according to the standard protocols with Vantana Benchmark automated stainer. Primary antibodies used in this study were monoclonal anti-α-DG (VIA4-1; Upstate Biotechnology, Lake Placid, NY, USA) and anti-β-DG (43DAG1/8D5; Novocastra Laboratories, Newcastle upon Tyne, UK) antibodies.

2.4. Immunoblotting and laminin overlay assay

The detailed techniques of immunoblotting, and laminin overlay assay have been described previously [31]. The following antibodies were used for immunoblotting analysis: monoclonal anti-α-DG (VIA4-1) and polyclonal anti-α-DG (GT20ADG, kindly provided by Prof. K. Campbell, Iowa Univ.), polyclonal anti-laminin-1 (Sigma, St. Louis, MO, USA), and monoclonal anti-β-DG (43DAG1/8D5).

2.5. Mutation analyses of α-DGP associated genes

Genomic DNA was extracted from leukocytes in peripheral blood lymphocytes according to standard protocols. All exons and their flanking intronic regions of *FKRP* (NM_024301.4), *FKTN* (NM_001079802.1), *POMGnT1* (NM_001243766.1), *POMT1* (NM_007171.3), *POMT2* (NM_013382.5), and *LARGE* (NM_004737.4) were amplified and sequenced using an automated 3100 DNA sequencer (Applied Biosystems, Foster, CA, USA). Primer sequences are available upon request. DNA samples from 100 Taiwanese individuals without apparent neuromuscular disorders were analyzed as controls.

3. Results

3.1. Patients with α-DGP caused by FKRP mutations

Seven of 50 patients with unclassified LGMD and CMD had a reduced α-DG immunoreaction using VIA4-1antibody, which recognizes glycosylated forms of α-DG on muscles, and they were thus considered to have α-dystroglycanopathy (Fig. 1). Among these seven patients, six had LGMD phenotype and one was CMD. Mutation screening revealed that five LGMD patients from four families harbored *FKRP* mutations (Fig. 2). No mutation in *FKTN*, *POMGnT1*, *POMT1*, *POMT2* and *LARGE* was identified in these seven patients. The clinical, pathological and biochemical information of all five patients with *FKRP* mutations are summarized in Table 1 together with that of a previously reported Taiwanese LGMD2I patient who was the first reported case in East-Asia (Patient 6) [26]. The c.948delC (p.Cys317Alafs*111) mutation was found heterozygously in four newly diagnosed patients (Patients 2, 3, 4 and 5) as well as in Patient 6. Patients 2, 3, and 4 carried a c.545A>G (p.TyrY182Cys) mutation, which was previously reported in two Brazilian patients, and a c.823C>T (p.Arg275Cys) mutation was identified in Patients 5 and 6. The compound heterozygous mutations for Patients 2, 5, and 6 were also found to lie on different parental alleles. Patient 1 bears two different novel

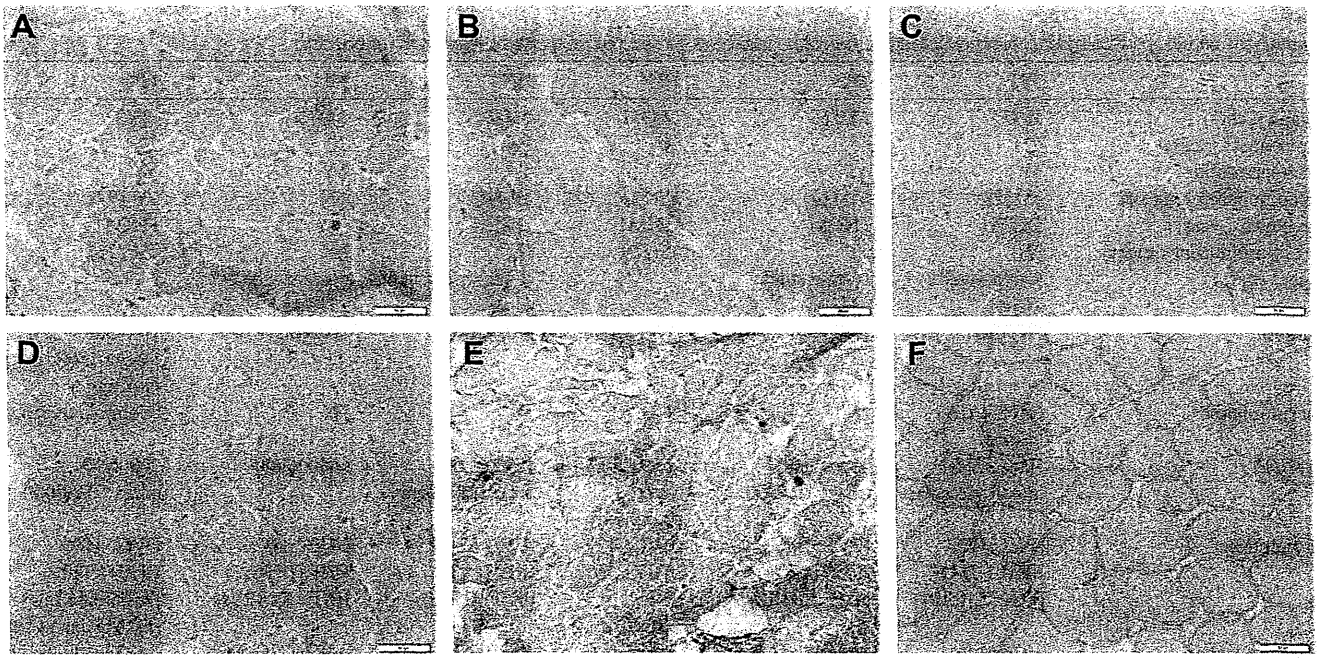

Fig. 1. Immunohistochemistry for α-DG (VIA4-1) in Patients 1, 2, 4, 5, and 6 (A–E). All patients' muscle samples showed markedly reduced staining, as compared with controls (F). Bar: 50 μm.

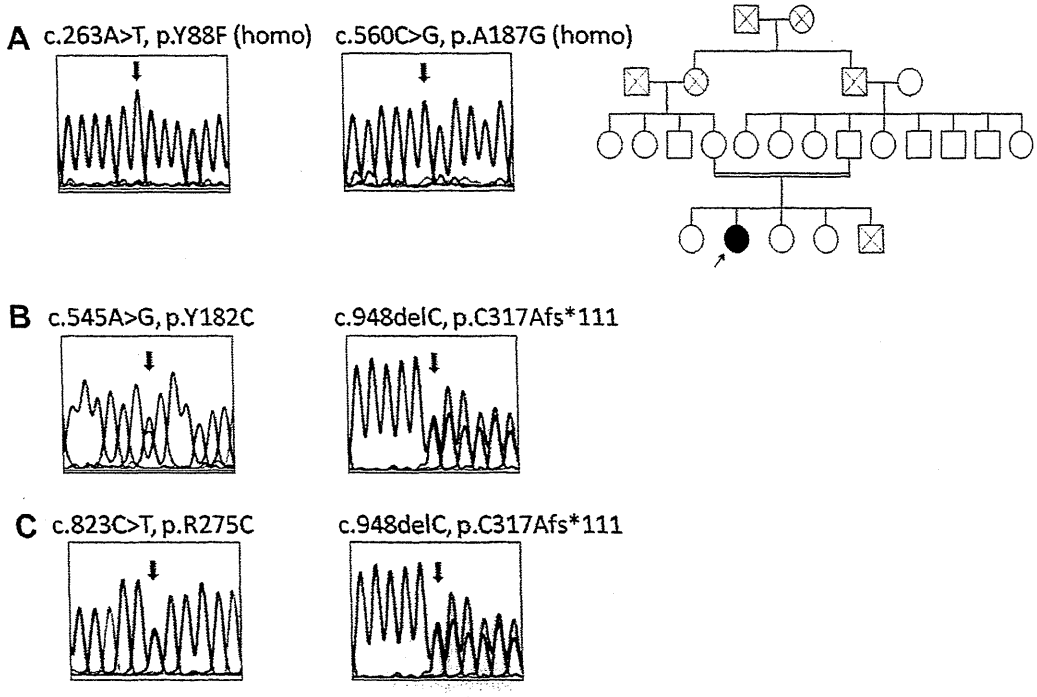

Fig. 2. Sequence analysis of *FKRP* revealed homozygous c.263A>T and c.560C>G mutations in Patient 1 (A), compound heterozygous c.545A>G and c.948delC mutations in Patients 2, 3, and 4 (B), and compound heterozygous c.823C>T and c.948delC mutations in Patients 5 and 6 (C). The pedigree of Patient 1 is also shown: the youngest brother of Patient 1 died of unknown causes at 7 months of age (A).

homozygous mutations, c.263A>T (p.Try88Phe) and c.560C>G (p.Ala187Gly), neither of which were identified in the human genome mutation database (HGMD) and 100 healthy individuals. The consanguineous healthy parents of Patient 1 carried these two missense mutations, heterozygously.

3.2. Reduced glycosylation of α-DG in LGMD2I patients

We further confirmed the altered glycosylation of α-DG in our LGMD2I patients (P2, 4, 5 and 6) using immunoblotting analysis and laminin overlay assay. On immunoblotting analysis using VIA4-1 antibody, skeletal

Table 1
Summary of clinical, pathological, biochemical and molecular analyses for the patients with α-dystroglycanopathy.

	P1	P2	P3[a]	P4[a]	P5	P6[b]
Sex/age (years)	F/35	M/16	M/31	M/30	M/10	F/23
Age of onset (years)	2	5	10	17	2	2
Calf hypertrophy	Y	Y	Y	Y	Y	Y
Cardiomyopathy (age of diagnosis, years)	Y (28) DCM	Y (14) DCM	Y (31) DCM	Y (30) DCM	N	Y (17) DCM
Loss of ambulatory ability (age, years)	N 6-min walk: 76 m	Y 6-min walk: 343 m	Y (29)	N 6-min walk: not done	N 6-min walk: 210 m	Y (12)
Cognition	Normal	Normal	Normal	Normal	Normal	Normal Brain MRI: negative finding
Other anomalies	Over-active bladder	N	N	N	N	Scoliosis with op
CK (IU/L)	1000–1500 max: unknown	4000–8000 max:>10,000	1500–2000 max: unknown	1500–2000 max: unknown	6000–9000	200–500 max: >10,000
Lung function	FVC: 32% FEV1: 33% PCF: 2.12 L/s	FVC: 45% FEV1: 53% PCF: 6.91 L/s	FVC: 43% FEV1: 36% PCF: 3.46 L/s	FVC: 62% FEV1: 73% PCF: 3.7 L/s	FVC: 64% FEV1: 76% PCF: 4.64 L/s	FVC: 10% FEV1: 12% PCF: 0.42 L/s BiPAP use at night
FKRP mutations	c.263A>T homo (F & M, hetero) c.560C>G homo (F & M, hetero)	c.545A>G (F, hetero) c.948delC (M, hetero)	c.545A>G c.948delC	c.545A>G c.948delC	c.823C>T (M, hetero) c.948delC (F, hetero)	c.823C>T (F, hetero) c.948delC (M, hetero)

Y: yes; N: nil; DCM: dilated cardiomyopathy; min: minute; m: meter; op: operation; max: maximum; F: Father; M: Mother.
[a] Siblings.
[b] Previously reported (Reference [21]).

muscles from all four patients showed fainter and smaller sized bands than the control (Fig. 3A). With GT20ADG antibody for the core region of α-DG, all skeletal muscles from these patients showed fainter broadbands with smaller molecular mass than that detected in the control (Fig. 3B). Laminin overlay assay displayed greatly reduced binding ability of α-DG to laminin in all patients (Fig. 3C).

3.3. Clinical findings of LGMD2I patients (Table 1)

The mean age of all 6 LGMD2I patients at examination was 24.2 ± 9.7 years, and the mean disease duration was 17.8 ± 9.1 years. The disease onset was variable, ranging from early childhood to late teens (2–17 years; 6.3 ± 6.1). All patients had calf hypertrophy and proximal dominant muscle weakness, starting from lower extremities and

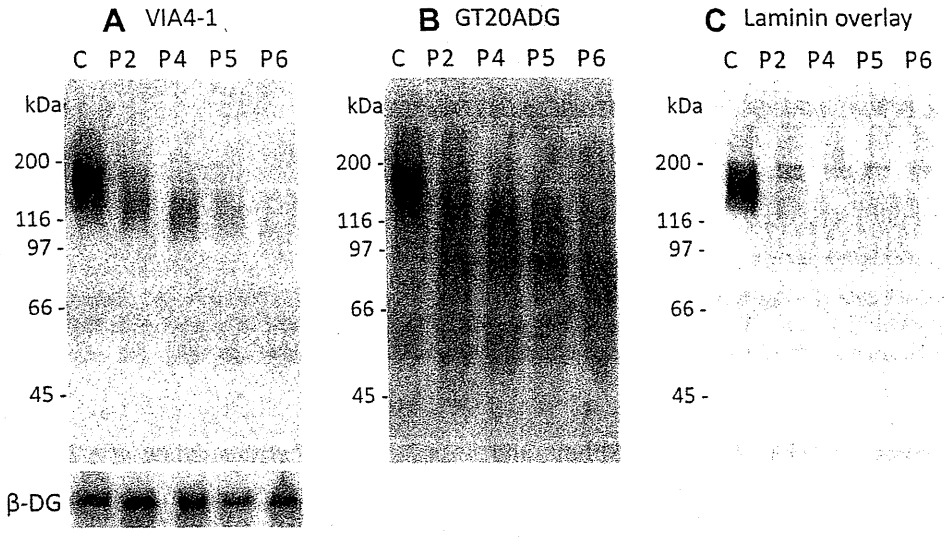

Fig. 3. Immunoblotting analysis. All 4 patients (P2, P4, P5 and P6) examined showed fainter and smaller sized bands than controls using α-DG (VIA4-1) (A). With the antibody of GT20ADG, fainter broadbands with smaller molecular weights were detected (B). Laminin overlay assay displayed greatly reduced binding ability of α-DG to laminin in all patients (C).

then extending to shoulder girdle and arms. Patient 2 became wheelchair-bound at the age of 29 years while Patient 6 lost her ambulatory ability at 14 years of age. Dilated cardiomyopathy (DCM) was seen in five of six patients (83.3%) and they are currently under medication. DCM was diagnosed with echocardiogram in Patients 2, 3, and 4 at their first visit to our hospital, so that the exact onset age of cardiac involvement was unclear. All patients had impaired pulmonary function with different degrees of severity but only Patient 6 required ventilator assistance (1 in 6; 16.7%). All patients had normal cognitive functions and the brain MRI of Patient 6 showed no notable abnormal changes. As for other abnormalities, only Patient 6 received an operation for scoliosis at 13 years of age. Serum creatine kinase levels were usually up to 10,000 IU/L at disease onset and then declined to hundreds at a later stage.

3.4. Muscle CT of LGMD2I patients

On muscle CT, all assessed patients (Patients 1–5) showed similar patterns of muscle involvement (Fig. 4) Lower extremities were more severely affected than upper extremities. Gluteus maximus was the most affected muscle (Fig. 4A), followed by posterior compartment of thigh muscles, among which biceps femoris and then adductors showed marked hypodensity (Fig. 4B). In the anterior compartment of thigh, vastus muscles and rectus femoris were equally involved. At the calf level, posterior compartment muscles, especially gastrocnemius and soleus, were also more affected than anterior part (Fig. 4C). As for upper extremities, involvement of shoulder girdle muscles including subscapularis, infraspinatus and supraspinatus was more prominent than trapezium and deltoid muscles (Fig. 4D).

4. Discussion

Wide variability in clinical picture has been reported in LGMD2I, of which the clinical features can be Duchenne muscular dystrophy-like, late-onset LGMD phenotypic and even asymptomatic [32,33]. In European countries, homozygosity of the most common missense mutation of c.826C>A (p.Leu276Ile) has been reported to confer a relatively milder phenotype than patients with compound heterozygous mutations [34]. A homozygous mutation of c.545A>G identified in the Brazilian patients has previously been reported to cause mild clinical phenotypes and disease course [32]. In our series, Patients 2–4 harbor the same compound heterozygous mutations of c.545A>G and c.948delC while Patients 5 and 6 both carry the same c.823C>T and c.948delC mutations. The patients carrying c.823C>T and c.948delC seem to show more severe clinical features than the patients having c.545A>G and c.948delC in terms of the age at onset, disease course, motor deterioration and complications. Because only a limited number of patients were included, however, additional patients with each mutation are required to clarify the phenotype and genotype correlation more clearly.

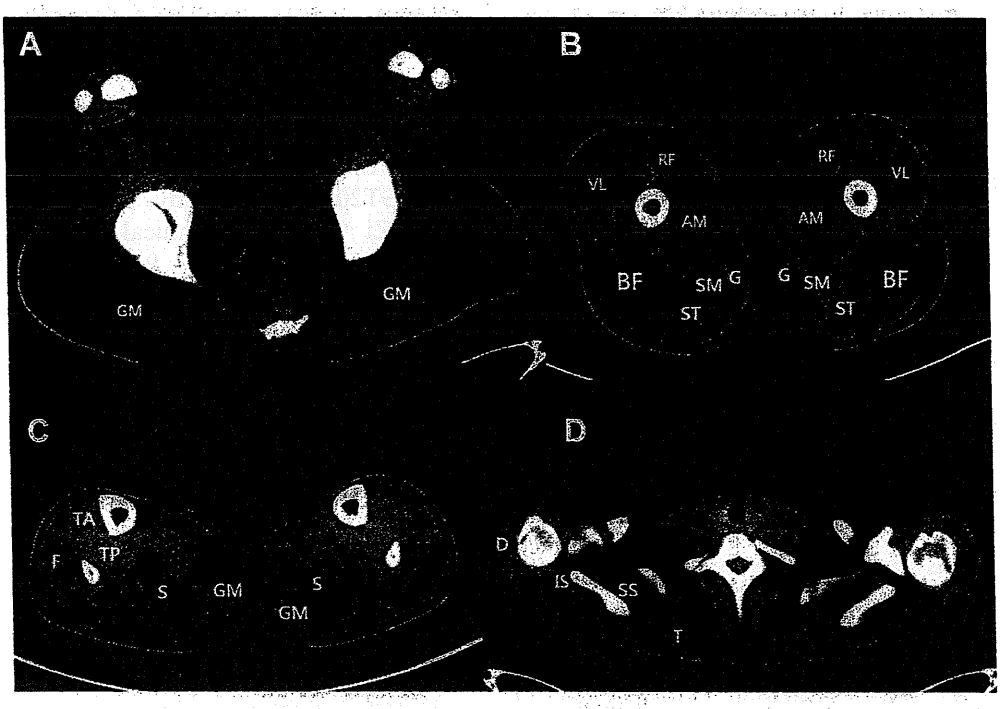

Fig. 4. Muscle CT on Patient 2. Gluteus maximus muscles were severely affected (A), followed by biceps femoris and adductors (B). At the calf level, gastrocnemius and soleus muscles were severely involved (C). In the upper extremities, involvement of subscapularis, infraspinatus and supraspinatus were more severe than trapezium and deltoid (D). (D: deltoid; IS: infraspinatus; SC: subscapularis; BF: biceps femoris; ST: semitendinosus; SM: semimembranous; S: soleus; F: fibularis; G: gastrocnemius; GM: gluteus maximus; RF: rectus femoris; VL: vastus lateralis; AM: adductor magus; G: gracilis).

Noteworthily, c.948delC in *FKRP* is a common mutation in Taiwanese LGMD2I patients. The mutation could cause frame shift and premature termination in translation (p.Cys317Alafs*111). We further screened 300 controls without neuromuscular diseases to determine the carrier frequency of c.948delC but none carried this mutation. This result suggests that the prevalence of the homozygosity of c.948delC is at least lower than 1 in 360,000, which may be too low to identify a homozygous patient. On the other hand, this result may also indicate that the homozygosity of this frame shift mutation is too severe to survive, since none of the homozygous null mutations in *FKRP* has been reported to date and *FKRP* knockout mice also showed embryonic lethality [35].

Interestingly, two different homozygous mutations, c.263A>T (p.Tyr88Phe) and c.560C>G (p.Ala187Gly), were found in Patient 1, but not in 100 controls. Her parents were consanguineous (cousins) and both harbored these two mutations heterozygously. Compared the amino acid sequences of the FKRP protein among different species, p.Tyr88 is highly conserved in mammals while p.Ala187 is preserved among primates and some mammals, but not in rodents. Furthermore, predictions of functional effects of these two variants using software showed that p.Tyr88Phe change is probably damaging but p.Ala187Gly is benign in terms of functional impact (http://genetics.bwh.harvard.edu/pph2/index.shtml). Accordingly, c.263A>T (p.Tyr88Phe) is more likely to be pathogenic in Patient 1 although further functional studies are still necessary.

In our cohort, cardiomyopathy accounted for 83% of our patients, whereas about 10–55% of European LGMD2I patients were reported to have cardiac problems [36]. As for respiratory function, only one of our patients (Patient 6) was ventilator-dependent at night although the other five developed variable degrees of respiratory impairment. However, the proportion of respiratory aid requirement was slightly lower than other reports [20, 36–38], probably because the assessment age and disease duration of our patients were also lower. Similar to previously reported LGMD2I patients, none of our patients had overt mental retardation.

So far few papers have focused specifically on the muscle imaging of LGMD2I patients [37,39]. Based on previous related literature, gluteal muscles and posterior compartment of thigh muscles were more affected than anterior compartment in LGMD2I. In our report, similar muscle involvement was seen on CT images in which gluteal maximus was the most severely affected, followed by adductors and biceps femoris. Some of these changes may overlap with those seen in other common LGMD, especially LGMD2A [39], such as the early involvement of gluteal muscles and predominant involvement of posterior compartment. However, selective involvement of medial gastrocnemius and soleus and relative sparing of vastus lateralis are characteristic for LGMD2A [12,21,40], which suggests that muscle images are still helpful for a differential diagnosis. In addition, different clinical phenotypes including commonly-seen calf hypertrophy and cardiac involvement in LGMD2I and the presence of characteristic lobulated fibers on muscle pathology of LGMD2A are also important to make the differentiation. In our series, all patients showed calf hypertrophy and 83% had cardiac problems; lobulated fibers were not observed in skeletal muscle from any patient and molecular analysis of *CAPN3* revealed no mutation.

LGMD2I is one of the most prevalent LGMD in Europe but is very rare in Asia. Only one from Taiwan (P6), two from China and another Asian patient from North America have been reported on thus far [26–28]. Also in Japan, only one LGMD2I patient was identified by the National Center of Neurology and Psychiatry, which has the largest muscle repository in Japan. Therefore, our report discloses that LGMD2I is not rare at least in Taiwan. Considering that the glycosylation defect may be too mild to be detected by immunohistochemical screening, there must be more LGMD2I patients who are as yet undiagnosed in Taiwan. Larger scale mutation analysis for uncategorized LGMD patients may be necessary for an early diagnosis of LGMD2I to be made. One common mutation, c.948delC, in the Taiwanese population may be associated with higher frequency and early development of cardiomyopathy although a larger number of patients is required to make this conclusive. However, it is still suggested that clinicians should closely monitor the cardiac function of LGMD2I patients harboring this mutation from late childhood or their early teens.

Acknowledgements

We thank Professor K.P. Campbell for kindly providing the GT20ADG antibody, Ms. Tzu-Min Kan and Ms. Wan-Zi Chen for technical assistance. This study was supported in part by 93-KMUH-048 from KMUH, intramural Research Grant 23-4, 23-5 for Neurological and Psychiatric Disorders from NCNP; in part by Research on Intractable Diseases, Comprehensive Research on Disability Health and Welfare, and Applying Health Technology from the Ministry of Health Labour and Welfare; and in part by the JSPS KAKENHI 24390227 and 24659437.

References

[1] Muntoni F, Brockington M, Blake DJ, Torelli S, Brown SC. Defective glycosylation in muscular dystrophy. Lancet 2002;360:1419–21.
[2] Toda T, Kobayashi K, Takeda S, et al.. Fukuyama-type congenital muscular dystrophy (FCMD) and alpha-dystroglycanopathy. Congenit Anom (Kyoto) 2003;43:97–104.
[3] Muntoni F, Torelli S, Brockington M. Muscular dystrophies due to glycosylation defects. Neurotherapeutics 2008;5:627–32.

[4] Mercuri E, Messina S, Bruno C, et al.. Congenital muscular dystrophies with defective glycosylation of dystroglycan: a population study. Neurology 2009;72:1802–9.
[5] Hara Y, Balci-Hayta B, Yoshida-Moriguchi T, et al.. A dystroglycan mutation associated with limb-girdle muscular dystrophy. N Engl J Med 2011;364:939–46.
[6] Beltran-Valero de Bernabe D, Currier S, Steinbrecher A, et al.. Mutations in the *O*-mannosyltransferase gene POMT1 give rise to the severe neuronal migration disorder Walker–Warburg syndrome. Am J Hum Genet 2002;71:1033–43.
[7] van Reeuwijk J, Janssen M, van den Elzen C, et al.. POMT2 mutations cause alpha-dystroglycan hypoglycosylation and Walker–Warburg syndrome. J Med Genet 2005;42:907–12.
[8] Yoshida A, Kobayashi K, Manya H, et al.. Muscular dystrophy and neuronal migration disorder caused by mutations in a glycosyltransferase, POMGnT1. Dev Cell 2001;1:717–24.
[9] Kobayashi K, Nakahori Y, Miyake M, et al.. An ancient retrotransposal insertion causes Fukuyama-type congenital muscular dystrophy. Nature 1998;394:388–92.
[10] Brockington M, Blake DJ, Prandini P, et al.. Mutations in the fukutin-related protein gene (FKRP) cause a form of congenital muscular dystrophy with secondary laminin alpha2 deficiency and abnormal glycosylation of alpha-dystroglycan. Am J Hum Genet 2001;69:1198–209.
[11] Longman C, Brockington M, Torelli S, et al.. Mutations in the human LARGE gene cause MDC1D, a novel form of congenital muscular dystrophy with severe mental retardation and abnormal glycosylation of alpha-dystroglycan. Hum Mol Genet 2003;12:2853–61.
[12] Roscioli T, Kamsteeg EJ, Buysse K, et al.. Mutations in ISPD cause Walker–Warburg syndrome and defective glycosylation of alpha-dystroglycan. Nat Genet 2012;44:581–5.
[13] Willer T, Lee H, Lommel M, et al.. ISPD loss-of-function mutations disrupt dystroglycan *O*-mannosylation and cause Walker–Warburg syndrome. Nat Genet 2012;44:575–80.
[14] Vuillaumier-Barrot S, Bouchet-Séraphin C, Chelbi M, et al.. Identification of mutations in TMEM5 and ISPD as a cause of severe cobblestone lissencephaly. Am J Hum Genet 2012;91:1135–43.
[15] Manzini MC, Tambunan DE, Hill RS, et al.. Exome sequencing and functional validation in zebrafish identify GTDC2 mutations as a cause of Walker–Warburg syndrome. Am J Hum Genet 2012;91:541–7.
[16] Buysse K, Riemersma M, Powell G, et al.. Missense mutations in β-1,3-N-acetylglucosaminyltransferase 1 (B3GNT1) cause Walker-Warburg syndrome. Hum Mol Genet 2013;22:1746–54.
[17] Lefeber DJ, de Brouwer AP, Morava E, et al.. Autosomal recessive dilated cardiomyopathy due to DOLK mutations results from abnormal dystroglycan *O*-mannosylation. PLoS Genet 2011;7:e1002427.
[18] Barone R, Aiello C, Race V, et al.. DPM2-DCG: a muscular dystrophy-dystroglycanopathy syndrome with severe epilepsy. Ann Neurol 2012;72:550–8.
[19] Lefeber DJ, Schönberger J, Morava E, et al.. Deficiency of Dol-P-Man synthase subunit DPM3 bridges the congenital disorders of glycosylation with the dystroglycanopathies. Am J Hum Genet 2009;85:76–86.
[20] Sveen ML, Schwartz M, Vissing J. High prevalence and phenotype–genotype correlations of limb girdle muscular dystrophy type 2I in Denmark. Ann Neurol 2006;59:808–15.
[21] Watanabe M, Kobayashi K, Jin F, et al.. Founder SVA retrotransposal insertion in Fukuyama-type congenital muscular dystrophy and its origin in Japanese and Northeast Asian populations. Am J Med Genet A 2005;138:344–8.
[22] Murakami T, Hayashi YK, Noguchi S, et al.. Fukutin gene mutations cause dilated cardiomyopathy with minimal muscle weakness. Ann Neurol 2006;60:597–602.
[23] Brockington M, Yuva Y, Prandini P, et al.. Mutations in the fukutin-related protein gene (FKRP) identify limb girdle muscular dystrophy 2I as a milder allelic variant of congenital muscular dystrophy MDC1C. Hum Mol Genet 2001;10:2851–9.
[24] Lim BC, Ki CS, Kim JW, et al.. Fukutin mutations in congenital muscular dystrophies with defective glycosylation of dystroglycan in Korea. Neuromuscul Disord 2010;20:524–30.
[25] Frosk P, Greenberg CR, Tennese AA, et al.. The most common mutation in FKRP causing limb girdle muscular dystrophy type 2I (LGMD2I) may have occurred only once and is present in Hutterites and other populations. Hum Mutat 2005;25:38–44.
[26] Lin YC, Murakami T, Hayashi YK, et al.. A novel FKRP gene mutation in a Taiwanese patient with limb-girdle muscular dystrophy 2I. Brain Dev 2007;29:234–8.
[27] Hong D, Zhang W, Wang W, Wang Z, Yuan Y. Asian patients with limb girdle muscular dystrophy 2I (LGMD2I). J Clin Neurosci 2011;18:494–9.
[28] Kang PB, Feener CA, Estrella E, et al.. LGMD2I in a North American population. BMC Musculoskelet Disord 2007;8:115.
[29] Yis U, Uyanik G, Heck PB, et al.. Fukutin mutations in non-Japanese patients with congenital muscular dystrophy: less severe mutations predominate in patients with a non-Walker-Warburg phenotype. Neuromuscul Disord 2011;21:20–30.
[30] Topaloglu H, Brockington M, Yuva Y, et al.. FKRP gene mutations cause congenital muscular dystrophy, mental retardation, and cerebellar cysts. Neurology 2003;60:988–92.
[31] Matsumoto H, Hayashi YK, Kim DS, et al.. Congenital muscular dystrophy with glycosylation defects of alpha-dystroglycan in Japan. Neuromuscul Disord 2005;15:342–8.
[32] de Paula F, Vieira N, Starling A, et al.. Asymptomatic carriers for homozygous novel mutations in the FKRP gene: the other end of the spectrum. Eur J Hum Genet 2003;11:923–30.
[33] Poppe M, Cree L, Bourke J, et al.. The phenotype of limb-girdle muscular dystrophy type 2I. Neurology 2003;60:1246–51.
[34] Mercuri E, Brockington M, Straub V, et al.. Phenotypic spectrum associated with mutations in the fukutin-related protein gene. Ann Neurol 2003;53:537–42.
[35] Chan YM, Keramaris-Vrantsis E, Lidov HG, et al.. Fukutin-related protein is essential for mouse muscle, brain and eye development and mutation recapitulates the wide clinical spectrums of dystroglycanopathies. Hum Mol Genet 2010;19:3995–4006.
[36] Poppe M, Bourke J, Eagle M, et al.. Cardiac and respiratory failure in limb-girdle muscular dystrophy 2I. Ann Neurol 2004;56:738–41.
[37] Bourteel H, Vermersch P, Cuisset JM, et al.. Clinical and mutational spectrum of limb-girdle muscular dystrophy type 2I in 11 French patients. J Neurol Neurosurg Psychiatry 2009;80:1405–8.
[38] Stensland E, Lindal S, Jonsrud C, et al.. Prevalence, mutation spectrum and phenotypic variability in Norwegian patients with limb girdle muscular dystrophy 2I. Neuromuscul Disord 2011;21:41–6.
[39] Fischer D, Walter MC, Kesper K, et al.. Diagnostic value of muscle MRI in differentiating LGMD2I from other LGMDs. J Neurol 2005;252:538–47.
[40] Wattjes MP, Kley RA, Fischer D. Neuromuscular imaging in inherited muscle diseases. Eur Radiol 2010;20:2447–60.

Available online at www.sciencedirect.com

SciVerse ScienceDirect

Neuromuscular Disorders 23 (2013) 441–444

www.elsevier.com/locate/nmd

Case report

Congenital generalized lipodystrophy type 4 with muscular dystrophy: Clinical and pathological manifestations in early childhood

Nobuyuki Murakami [a,b,*], Yukiko K. Hayashi [b,c], Yuji Oto [a], Masahisa Shiraishi [a], Hisashi Itabashi [a], Kyoko Kudo [d], Ichizo Nishino [b,c], Ikuya Nonaka [b], Toshiro Nagai [a]

[a] *Department of Pediatrics, Dokkyo Medical University, Koshigaya Hospital, Koshigaya, Saitama, Japan*
[b] *Department of Neuromuscular Research, National Institute of Neuroscience, National Center of Neurology and Psychology, Kodaira, Tokyo, Japan*
[c] *Department of Clinical Development, Translational Medical Center, National Center of Neurology and Psychology, Kodaira, Tokyo, Japan*
[d] *Department of Pediatrics, Saitama Municipal Hospital, Saitama, Japan*

Received 17 August 2012; received in revised form 28 December 2012; accepted 6 February 2013

Abstract

A boy with congenital generalized lipodystrophy type 4 with muscular dystrophy presented in infancy with delay in motor milestones and a persistent elevation of CK. There was no associated mental retardation. He was followed up to 3 years and 11 months; he had a homozygous c.696_697insC mutation in *polymerase I and transcript release factor* (PTRF). He started to walk at 2 years and 6 months although he did not have mental retardation. Insulin resistance appeared at 3 years and 11 months of age. PTRF immunostaining positivity was absent in the muscle but caveolin-3 was preserved in the sarcolemma at 16 months of age. Secondary deficiency of caveolins may be closely associated with disease progression.

Keywords: PTRF; Generalized lipodystrophy; Muscular dystrophy; Insulin resistance; Muscle mounding

1. Introduction

Congenital generalized lipodystrophies are rare autosomal recessive disorders that are characterized by an almost total loss of subcutaneous adipose tissues from birth, insulin resistance, diabetes, hypertriglyceridemia, and hepatic steatosis [1,2]. Recently, we first described muscular dystrophy with generalized lipodystrophy caused by *polymerase I and transcript release factor* (PTRF) mutations [3], and this disease was categorized as congenital generalized lipodystrophy type 4 (CGL4) (OMIM #613327). Patients with PTRF deficiency can show various symptoms that include arrhythmia, atlantoaxial instability, and pyloric stenosis in addition to manifestations of congenital generalized lipodystrophy and muscular dystrophy [3–6].

Only a limited number of patients with this condition have been reported. Therefore, the accumulation of detailed clinical information, especially in early childhood, is important to understand this disease and to facilitate early diagnosis. Herein, we describe the detailed clinical course of a 3-year-old Japanese boy with CGL4 with muscular dystrophy.

2. Case report

Our patient was a Japanese boy aged 3 years and 11 months from healthy non-consanguineous parents. He was born via normal delivery at 39 weeks and 4 days of gestational age. His body height, body weight, and head circumstance were 47 cm (−1.0 SD), 3070 g (−0.3 SD), and 34 cm (0.3 SD), respectively. He gained body weight

* Corresponding author. Address: Department of Pediatrics, Dokkyo Medical University, Koshigaya Hospital, 2-1-50 Minami-Koshigaya, Koshigaya, Saitama 343-8555, Japan. Tel.: +81 48 965 1111; fax: +81 965 8363.
E-mail address: nobuyuki@dokkyomed.ac.jp (N. Murakami).

0960-8966/$ - see front matter © 2013 Elsevier B.V. All rights reserved.
http://dx.doi.org/10.1016/j.nmd.2013.02.005

slowly and weighed 4.5 kg at 4 months of age, upon which he was diagnosed with hypothyroidism. An elevated serum creatine kinase (CK) level (812 IU/L; normal <200) was also noted. He received thyroid hormone therapy consisting of 10 μg/day levothyroxine sodium hydrate. The subcutaneous fat of his face began to decrease at 7 months of age. He was referred to our hospital at 11 months of age because of continuous elevation of serum CK levels. Although he had head control at 4 months of age, he showed delayed motor milestones. He could crawl at 14 months and sit at 16 months of age. He showed normal mental development and spoke several meaningful words at 14 months of age.

At 16 months of age, his body height and weight were 78.5 cm (−0.1 SD) and 9.6 kg (−0.5 SD), respectively. He had a saddle nose, prominent ears, curled hair, and mild macroglossia. Loss of subcutaneous fat was marked on his face and limbs, which exposed prominent blood vessels in his extremities. His abdomen was distended without evidence of hepatosplenomegaly or tumor. He did not have hypertrophic tonsils or scoliosis and facial muscle involvement or a high arched palate was not observed. He had mild hypertrophic muscles, especially in his extremities, and mild proximal muscle weakness was seen with normal deep tendon reflexes. He could crawl and stand with support. Although he demonstrated percussion-induced muscle mounding, he did not demonstrate the rippling phenomenon.

His serum CK level had increased to 2293 IU/L, but his serum immunoglobulin level was normal. Chest radiography, electrocardiography, cardiac echocardiography, and bone radiography showed normal findings. A muscle computed tomography (CT) showed decreased subcutaneous adipose tissue and hypertrophic muscles with normal intensity (Fig. 1A).

A muscle biopsy taken from his left biceps brachii showed dystrophic changes including variation in fiber size and scattered necrotic and regenerating fibers (Fig. 2A and B). Immunohistochemistry for PTRF was negative in both the sarcolemma of the muscle fibers and blood vessels (Fig. 2C). The caveolin-3 stain was slightly irregular but well preserved (Fig. 2D), whereas the immunoreactions of caveolins-1 and -2 were barely detectable in the blood vessels (data not shown). Antibodies for dystrophin and other major proteins associated with muscular dystrophies showed normal staining (data not shown). Genetic analysis revealed a homozygous mutation of c.696_697insC in the *PTRF* gene, which is a common mutation in Japanese CGL4 patients [3]. This mutation resulted in substitution of the last 158 amino acids with an unrelated 191-amino acid sequence; moreover, the mutant protein was mislocalized, as shown by a previous *in vitro* experiment [3].

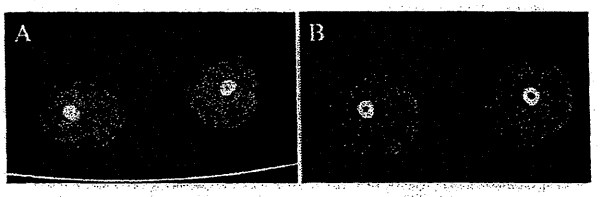

Fig. 1. Computed tomographic scan at the thigh level at 1 year (A) and 2 years and 10 months (B) of age. The thigh muscles showed hypertrophy without abnormal intensity. Note the progressive loss of subcutaneous adipose tissues.

He started to walk without support at 2 years and 6 months of age and he could speak 2-word sentences. At the age of 2 years and 10 months, his body height and weight were 92.7 cm (+0.2 SD) and 13.2 kg (−0.1 SD), respectively (Table 1). He could run and climb stairs slowly, but he could not jump. The Gowers' sign was negative. The endocrinological examination results at that time were as follows: total cholesterol (T-cho), 213 (140–220) IU/L; triglyceride (TG), 309 (30–150) mg/dL; high-density lipopolysaccharide cholesterol (HDL-C), 27 (40–76) mg/dL; low-density lipopolysaccharide cholesterol (LDL-C), 125 (70–139) mg/dL; glucose, 98 mg/dL; HbA1c, 5.1 (3.8–5.5)%; insulin, 1.5 (5.0–20.0) μU/mL; fT4, 1.42 (0.97–1.80) ng/dL; fT3, 4.36 (2.73–4.50) pg/mL; and thyroid-stimulating hormone, 4.560 (0.300–3.000) μU/mL. The oral glucose tolerance test showed a normal reaction and his blood sugar level was 123 mg/mL 2 h after administration. The calculated insulin resistance index (HOMA-R) was 1.24 (<1.6). Serum adiponectin, total PAI-1, and leptin levels were 1.2 (>4.0) μg/mL, 23 (<50) ng/mL, and 1.9 (male: 0.9–13.0, female: 2.5–21.8) ng/mL, respectively.

At 3 years and 11 months of age, his body height and weight were 99.2 cm (−0.1 SD) and 15.3 kg (−0.1 SD), respectively. The endocrinological examination results at that time were as follows: T-cho, 154 IU/L; TG, 680 mg/dL; HDL-C, 20 mg/dL; LDL-C, 57 mg/dL; glucose, 98 mg/dL; HbA1c, 5.0%; and insulin, 12.3 μU/mL. His HOMA-R was increased to 2.98. Serum adiponectin, total PAI-1, and leptin levels were 1.1 μg/mL, 96 ng/mL, and 1.6 ng/mL, respectively. His body fat percentage was 12.2% according to dual energy X-ray absorptiometry (DEXA) measurement.

3. Discussion

We previously reported that the clinical features observed in patients with *PTRF* mutations were closely associated with a secondary deficiency of caveolin [3].

In various types of congenital generalized lipodystrophy, body fat loss and insulin resistance are usually noticed at birth. In CGL4, however, the loss of adipose tissue in the face is observed after several months of age and insulin resistance appears from early childhood [3–6]. The boy described herein showed decreased subcutaneous fat in his face at 7 months of age. Lipodystrophy was progressive, and loss of adipose tissue in the lower legs became more apparent with age. This finding was confirmed by CT images. Metabolic

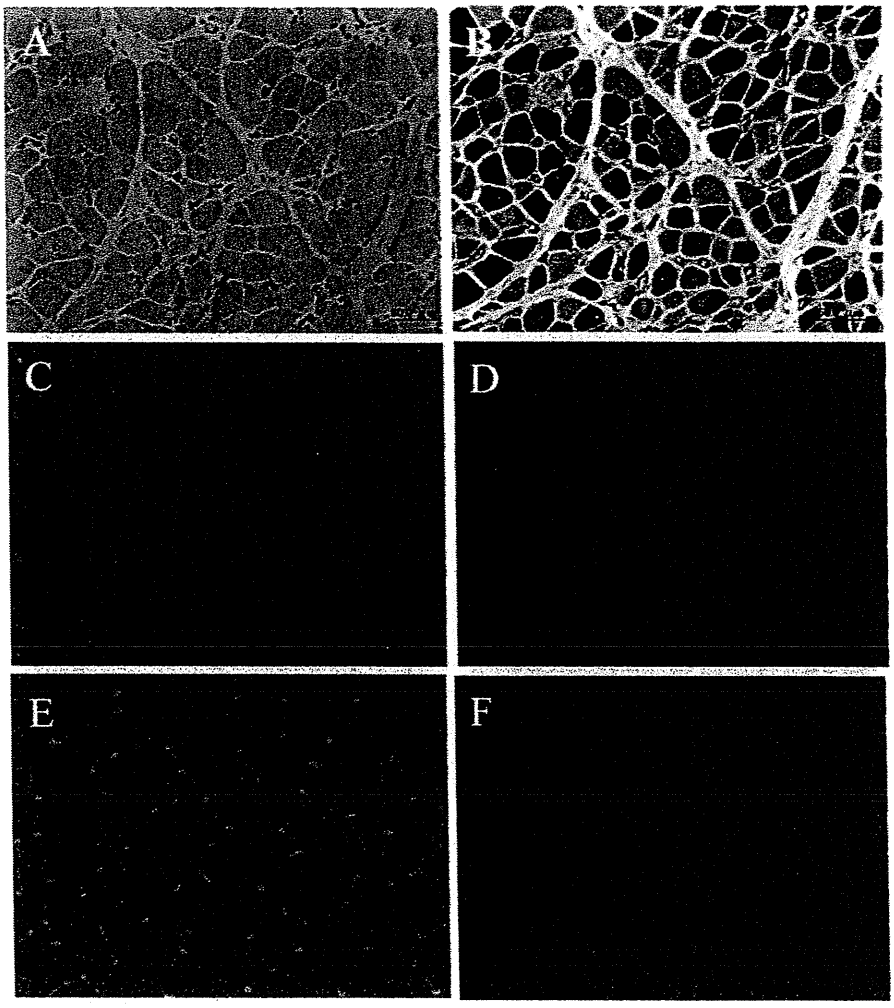

Fig. 2. The biceps brachii muscle showed moderate variation in fiber size, a few necrotic fibers, and increased endomysial and perimysial fibrosis (A, B). Negative immunoreactivity for PTRF (C) but almost normal caveolin-3 levels was observed (D). A: hematoxylin and eosin stain. B: NADH-tetrazolium reductase stain. C, E: PTRF immunohistochemistry. D, F: caveolin-3 immunohistochemistry. E, F: control muscle. Scale bar: 50 μm.

abnormalities were also progressive. Although he did not have insulin resistance at 2 years and 10 months of age, he already showed high levels of T-cho and TG. He demonstrated insulin resistance at 3 years and 11 months.

PTRF is an essential component for the stabilization of caveolae. PTRF-deficient mice do not have detectable caveolae and show decreased insulin receptor levels in fat tissue [10]. Similarly, caveolin-1-deficient mice that show loss of caveolae have been reported to show insulin resistance due to decreased insulin receptor levels in adipose tissues [7–9]. This and a previous report [3] have shown that caveolin-1 and caveolin-2 levels greatly reduced in the intramuscular blood vessels from PTRF-deficient patients. Lipodystrophy and insulin resistance can be closely associated with secondary deficiency of caveolins.

This boy had delayed motor milestones associated with dystrophic changes in his muscles. Interestingly, sarcolemmal caveolin-3 staining was well preserved in this patient compared to previously reported results in older patients, although his immunoreactivity for PTRF was defective. In the case of a 3-year-old Japanese girl who did not show muscle weakness accompanied by high serum levels of CK [5], caveolin-3 immunoreactivity was well preserved despite negative reactivity of PTRF. Secondary reduction of caveolin-3 may progress with age or disease progression [3]; and further studies are necessary to confirm this.

Percussion-induced muscle mounding is a characteristic finding in patients with PTRF deficiency as well as in some patients with caveolin-3 deficiency. Although the detailed mechanism involved in muscle mounding remains to be elucidated, it may be closely related to deficiencies of both caveolin-3 and PTRF.

CGL4 with muscular dystrophy is a progressive disorder, and cardiac problems, including arrhythmia,

Table 1
Clinical and biological summary.

Age	Height (SD)	Weight (SD)	Clinical and biological signs	CK (normal < 200 IU/L)	T-Cho (140–220 IU/L)	TG (30–150 mg/dL)	Adiponectin (>4.0 μg/mL)	Leptin (0.9–13.0 ng/mL)
Birth	47.0 cm (−1.0)	3.1 kg (−0.3)	Normal amount of subcutaneous fat	ND	ND	ND	ND	ND
4 m	59.0 cm (−2.3)	4.5 kg (−2.9)	Head control (+), hypothyroidism	812	ND	ND	ND	ND
7 m	66.4 cm (−1.2)	5.8 kg (−2.7)	Deceased subcutaneous fat on his face	1779	ND	ND	ND	ND
14 m	76.2 cm (−0.3)	8.6 kg (−1.2)	Crawl (+), stand with support (+), meaningful words (+)	1973	ND	ND	ND	ND
16 m	78.5 cm (−0.1)	9.6 kg (−0.5)	Sit alone (+), loss of subcutaneous fat on his face and extremities	2293	252	ND	ND	ND
2 y 6 m	88.0 cm (−0.5)	12.9 kg (+0.2)	Walk alone (+), 2-word sentences (+)	ND	ND	ND	ND	ND
2 y 10 m	92.7 cm (+0.2)	13.2 kg (−0.1)	Run (+), jump (−), normal glucose tolerance and no insulin resistance, low level of adipokines	1715	213	309	1.2	1.9
3 y 11 m	99.2 cm (−0.1)	15.3 kg (−0.1)	Insulin resistance (+)	1777	154	680	1.1	1.6

ND: not done.

supraventricular, and ventricular tachycardia, may develop after 8–10 years of age [3,4,6]. Careful follow-up is necessary for a better prognosis.

Acknowledgements

This study was supported partly by Intramural Research Grants 23-4, 23-5 for Neurological and Psychiatric Disorders of NCNP; partly by Research on Intractable Diseases, Comprehensive Research on Disability Health and Welfare, and Applying Health Technology from the Ministry of Health Labour and Welfare; and partly by JSPS KAKENHI. Grant Numbers 24390227 and 24659437.

References

[1] Garg A, Agarwal AK. Lipodystrophies: disorders of adipose tissue biology. Biochim Biophys Acta 2009;1791:507–13.
[2] Garg A. Lipodystrophies: genetic and acquired body fat disorders. J Clin Endocrinol Metab 2011;96:3313–25.
[3] Hayashi YK, Matsuda C, Ogawa M, et al. Human *PTRF* mutations cause secondary deficiency of caveolins resulting in muscular dystrophy with generalized lipodystrophy. J Clin Invest 2009;119:2623–33.
[4] Rajab A, Straub V, McCann LJ, et al. Fatal cardiac arrhythmia and long-GT syndrome in a new form of congenital generalized lipodystrophy with muscle rippling (CGL4) due to *PTRF-CAVIN* mutations. PLoS Genet 2010;6:e1000874.
[5] Dwianingsih EK, Takeshima Y, Itoh K, et al. A Japanese child with asymptomatic elevation of serum creatine kinase shows PTRF–Cavin mutation matching with congenital generalized lipodystrophy type 4. Mol Genet Metab 2010;101:233–7.
[6] Shastry S, Delgado MR, Dirik E, Mehmet T, Agrarwal AK, Garg A. Congenital generalized lipodystrophy, type 4 (CGL4) associated with myopathy due to novel *PTRF* mutations. Am J Med Genet A 2010;152A:2245–53.
[7] Ranzani B, Combs TP, Wang XB, et al. Cavoline-1-deficient mice are lean, resistant to diet-induced obesity, and show hypertriglyceridemia with adipocyte abnormalities. J Biol Chem 2002;277:8635–47.
[8] Cohen AW, Razani B, Wang XB, et al. Caveolin-1-deficient mice show insulin resistance and defective insulin receptor protein expression in adipose tissue. Am J Physiol Cell Physiol 2003;285:c222–35.
[9] Gnozález-Muñoz E, López-Iglesias C, Calvo M, Palacín M, Zorzano A, Camps M. Cavolin-1 loss of function accelerates glucose transporter 4 and insulin receptor degradation in 3T3-L1 adipocytes. Endocrinology 2003;150:3493–502.
[10] Liu L, Brown D, McKee M, et al. Deletion of Cavin/PTRF causes global loss of caveolae, dyslipidemia and glucose intolerance. Cell Metab 2008;8:310–7.

Journal of Neuroscience Research

Journal of Neuroscience Research 92:287–297 (2014)

Enhanced Prepulse Inhibition and Low Sensitivity to a Dopamine Agonist in Hesr1 Knockout Mice

Kouta Kanno,[1,2] Hiroki Kokubo,[3,4,5] Aki Takahashi,[4,6] Tsuyoshi Koide,[4,6] and Shoichi Ishiura[1,2]*

[1]Department of Life Sciences, Graduate School of Arts and Sciences, The University of Tokyo, Tokyo, Japan
[2]2Department of Biological Sciences, Graduate School of Science, The University of Tokyo, Tokyo, Japan
[3]Division of Mammalian Development, National Institute of Genetics, Mishima, Shizuoka, Japan
[4]The Graduate University for Advanced Studies (SOKENDAI), Hayama, Japan
[5]Cardiovascular Physiology and Medicine, Division of Molecular Medical Science, Graduate School of Biomedical Sciences, Hiroshima University, Hiroshima, Japan
[6]Mouse Genomics Resource Laboratory, National Institute of Genetics, Mishima, Shizuoka, Japan

Transcription factor Hesr family genes are important in neuronal development. We demonstrated previously that HESR1 and HESR2 modified expression of the dopamine transporter (DAT) reporter gene. HESR-family genes have been investigated in development, but their functions, especially in relation to behaviors regulated by dopamine, in adult animals remain unclear. In the present study, we investigated the effects of Hesr1 and Hesr2 on behavior. A behavioral test battery to examine spontaneous activity, anxiety-like behavior, aggressive behavior, pain sensitivity, and sensorimotor gating was conducted in Hesr1 and Hesr2 knockout (KO) mice. Enhanced prepulse inhibition (PPI), which is a form of sensorimotor gating, was observed in only Hesr1 KO mice; other behavioral traits were mostly comparable to wild-type animals in both the Hesr1 and the Hesr2 KO lines. Next, we used a dopamine agonist, apomorphine, to confirm the involvement of the dopaminergic system. Injection of apomorphine reduced the enhanced PPI in Hesr1 KO mice. Additionally, dose-dependent sensitivity to the agonist was lower in the Hesr1 KO mice than in wild-type mice, suggesting that the enhanced PPI resulted from this alteration in dopamine sensitivity. Furthermore, DAT mRNA was downregulated in Hesr1 KO mice, whereas the dopamine D1 and D2 receptors were comparable. These findings suggest Hesr1 to be a novel factor that affects dopamine sensitivity and the sensorimotor gating system.

Key words: Hesr1; Hesr2; dopamine transporter; dopamine receptor; apomorphine

The Hesr (hairy/enhancer of split-related transcriptional factor with YRPW motif)-family genes Hesr1, −2, and −3 (Hey1, Hey2, and HeyL) were identified as hairy/enhancer split-type basic helix-loop-helix (bHLH) genes and have been shown to be direct transcriptional targets of the Notch signaling pathway, which is essential for neural development (Kokubo et al., 1999; Leimeister et al., 1999; Nakagawa et al., 1999; Henderson et al., 2001; Iso et al., 2001, 2003; Wang et al., 2002; Sakamoto et al., 2003). Recently, it was also reported that HESR1 was upregulated in cell lines derived from patients with autism-spectrum disorder, thought to be a neurodevelopmental disorder (Seno et al., 2011). Furthermore, HESR1 mediates activation of p53 (Villaronga et al., 2010), which has been reported to be a schizophrenia susceptibility gene (Allen et al., 2008). Thus, HESRs seem to be important for not only normal development but also psychiatric and neurodevelopmental disorders. However, their functions, especially related to behavior in adults, remain unclear.

We previously identified and characterized HESR1 as a trans-acting repressor of gene expression that binds to

Additional Supporting Information may be found in the online version of this article.

Contract grant sponsor: Human Frontier Science Program; Contract grant sponsor: Ministry of Health, Labor and Welfare, Japan; Contract grant sponsor: Ministry of Education, Culture, Sports, Science, and Technology of Japan; Contract grant sponsor: JSPS (to K.K.).

K. Kanno's current address is Japan Society for Promotion of Science, Companion Animal Research, School of Veterinary Medicine, Azabu University, Room 303, Bldg 7, 1-17-71 Fuchinobe, Sagamihara, Kanagawa 252-5201, Japan

*Correspondence to: Dr. Shoichi Ishiura, Department of Life Sciences, Graduate School of Arts and Sciences, The University of Tokyo, 3-8-1 Komaba, Meguro-ku, Tokyo 153-8902, Japan. E-mail: cishiura@mail.ecc.u-tokyo.ac.jp

Received 14 May 2013; Revised 17 July 2013; Accepted 31 July 2013

Published online 25 November 2013 in Wiley Online Library (wileyonlinelibrary.com). DOI: 10.1002/jnr.23291

the 3′-untranslated region (UTR) of the dopamine transporter (DAT) gene (Fuke et al., 2005, 2006). We also demonstrated that not only HESR1 but also HESR2 reduced DAT reporter gene expression, which contains the human DAT 3′-UTR (Kanno and Ishiura, 2011). The dopaminergic nervous system plays important roles in locomotion, cognition, reward, emotion, and hormone release (Jackson and Westlinddanielsson, 1994; Missale et al., 1998; Bannon et al., 2001; Uhl, 2003). Polymorphisms in dopamine-related genes, such as those responsible for the expression of dopamine receptors, tyrosine hydroxylase (TH), and the human dopamine transporter (DAT1, SLC6A3), have been reported to be associated with human neuropsychiatric disorders and behavior (D'Souza and Craig, 2008). For example, the 3′-UTR of exon 15 in DAT1 contains a 40-bp-long variable number of tandem repeats (VNTR; Vandenbergh et al., 1992; Michelhaugh et al., 2001). This VNTR polymorphism is known to be associated with neuropsychiatric disorders such as attention-deficit hyperactivity disorder (ADHD), Parkinson's disease (PD), alcoholism, and drug abuse (Cook et al., 1995; Ueno et al., 1999; Vandenbergh et al., 2000; Ueno, 2003; D'Souza and Craig, 2008). It is involved in modified gene expression both in vivo (Heinz et al., 2000; Jacobsen et al., 2000; Mill et al., 2002; D'Souza and Craig, 2008) and in mammalian cell lines (Fuke et al., 2001, 2005; Inoue-Murayama et al., 2002; Miller and Madras, 2002; Greenwood and Kelsoe, 2003; Mill et al., 2005; VanNess et al., 2005; D'Souza and Craig, 2008). Thus, the relationship between HESRs and the dopaminergic system seems worthy of discussion.

The present study seeks to clarify the behavioral function(s) of Hesr1 and Hesr2. We first examined altered behavior in knockout (KO) mice compared with their wild-type counterparts using a series of behavioral tests. Furthermore, dopamine-related gene expression in the brains of KO mice was analyzed. Finally, we used a dopamine agonist to confirm functional alteration of the dopaminergic system in the KO mice.

MATERIALS AND METHODS

General Procedures

Hesr1 KO and Hesr2 KO mice were subjected to a behavioral test battery to determine their functions. Additionally, real-time quantitative PCR analyses and Western blotting were performed to quantify the expression of dopamine-related genes in the KO mice: DAT, TH (a marker of dopaminergic neurons), and dopamine D1 (D1) and D2 receptors (D2). Involvement of the dopaminergic system was also investigated pharmacologically in terms of behaviors for which scores in the battery were statistically different from those of wild-type mice.

Animals

Male Hesr1 and Hesr2 KO mice and each littermate wild-type strain with C57BL/129Svj backgrounds (Kokubo et al., 2005) were used. Their ages were 8 to 16 weeks when the behavioral test began. All animals were housed in standard mouse cages with free access to food and water at the National Institute of Genetics (NIG) under a 12/12-hr light/dark cycle (lights on from 06:00 to 18:00 hr) in a temperature-controlled room (23°C ± 2°C). The mice were housed with their littermates before the tests and singly during the tests. All behavioral assays were conducted during the light period. Mice were maintained according to NIG guidelines. All procedures were approved by the Institutional Committee for Animal Care and Use.

Behavioral Test Battery

A series of behavioral tests comprising 10 kinds of observations were conducted in a previously determined order (Table I). This battery was composed of behavioral tests for mainly the measurement of spontaneous activity, emotionality including anxiety and aggressiveness, and sensorimotor gating, in addition to those for motor control and nociception. The body weight of each mouse was measured after the open field test. The number of animals used is indicated in the Table I footnote.

Novel Cage Test

Individual spontaneous activity was recorded for 1 hr with an infrared sensor (Activity Sensor; Ohara Co. Ltd., Tokyo, Japan) immediately after each mouse had been transferred to the novel home cage (novel surroundings). This sensor was located above the lid (made from stainless-steel wire) of each cage. The sensor records the motion of the mouse inside the home cage as counts by the sensor (Nishi et al., 2010). With this apparatus, many kinds of activity, such as horizontal locomotion, climbing the cage lid, hanging on the lid, and jumping, could be detected and were taken to represent the total activity. The activity of each 1-min bin was measured as accumulated counts if the animal was active in any area of the cage.

Home Cage Test

Using the same system as that in the novel cage test described above, spontaneous activity was recorded in the same cages directly after the novel cage test. The activity in each 1-min bin was measured as accumulated counts if the animal was active in any area of the cage. The activity counts over 72 hr were summed, and the total activity scores were the average counts for a 1-day period over 3 days. Total activity was divided into two components, active time and average activity. Active time was calculated as the total number of minutes in which the mouse accumulated more than one count within a 1-min interval. Thus, the active time estimated the approximate duration of movement. Average activity, which was an index of the intensity of activity, was calculated using the following formula: average activity = total activity/active time. The average activity reflected the average amount of locomotion in 1 min of active time.

Open Field Test

Anxiety-like behaviors were assessed by open field tests ("total time in center area" in Table I) as well as spontaneous activity ("total distance"), similar to our previous reports (Takahashi et al., 2006, 2008). The open field used consisted of a square arena (60 × 60 × 40 cm) made of a white polyvinylchloride

plastic board that was divided into 16 equal squares. The arena was brightly lit by incandescent lighting (365 lux).

To analyze ambulation length ("total distance" in Table I), central ambulation and time spent in the center ("total time in center" in Table I), the arena was recorded continuously with a video camera placed over its center and relayed to a video tracking system (Image OF; Ohara Co. Ltd.) based on the National Institutes of Health (NIH) ImageJ software.

Light–Dark Box Test

Anxiety-like behaviors were assessed using the light–dark box test ("time in light area" and "latency of transition" in Table I) as well as spontaneous activity ("No. of times of transition"), similar to our previous report (Takahashi et al., 2008) and a traditionally important test (Crawley and Goodwin, 1980). The apparatus (Scanet MV-10 and MV-20; Melquest Co., Ltd., Toyama, Japan) consisted of coupled black and transparent acrylic chambers (each measuring 15 × 15 × 16 cm) separated by a black acrylic board with an aperture of 4-cm diameter between them. To start the measurement, mice were placed individually into the dark chamber (0 lux). Then, the latency of the first transition into the light chamber (95 lux), number of transitions between light and dark chambers, and time spent in the light chamber were measured for 10 min.

Elevated Plus Maze Test

Anxiety-like behaviors were assessed using the elevated plus maze test ("open arm entry/total entry" in Table I) as well as spontaneous activity ("total distance"), similar to our previous reports (Takahashi et al., 2008) and a traditionally important test (Pellow et al., 1985). The apparatus, made of a white acrylic board, consisted of two open arms with low edges (30 × 5 × 0.25 cm) and two closed arms enclosed by a clear acrylic plastic wall (30 × 5 × 15 cm) that extended from a central platform (5 × 5 cm). It was elevated 60 cm above the floor and was dimly lit (150 lux). Mice were individually placed in the center platform and allowed to move freely for 10 min. Ambulatory activity (total distance), the number of entries into the open or closed arms, and duration in the open or closed arms were measured using a video tracking system (Image EPM; Ohara Co. Ltd.) based on the NIH ImageJ software.

Resident–Intruder Test

Aggression was observed using the resident–intruder paradigm, which is a widely used and traditional test in rodents (Miczek and O'Donnell, 1978). C57BL6/J mice (maintained at NIG) that were younger than the subject males were used as intruders. An intruder mouse was put into the home cage of the subject, and the aggressive behavior of the subject (resident) mouse was observed. Latency of first attack bite and the number of bites from residents to intruders were observed for 15 min. All tests were recorded with a video camera.

Rota-Rod Test

Motor control was assessed using the rota-rod test, which has been traditionally used for rodents (Jones and Roberts,

TABLE I. Summary of Behavioral Test Battery*

Schedule	Tests	Index	Hesr1(+/+)	Hesr1(−/−)	Significance	Hesr2(+/+)	Hesr2(−/−)	Significance
1 Day 1	Novel-cage test	Total activity	1,640.1 ± 149.5	1,710.8 ± 183.1	n.s. (*t*-test)	1,239.1 ± 159.2	1430.3 ± 135.7	n.s. (*t*-test)
2 Days 2–5	Home-cage test	Total activity	34,918.5 ± 2,551.5	30,835.0 ± 1610.3	n.s. (Wilcoxon)	27,718.6 ± 2,773.4	29,951.6 ± 2,985.3	n.s. (Wilcoxon)
		Total active time (min)	1,576.5 ± 71.3	1,514.1 ± 73.6	n.s. (*t*-test)	1,370.8 ± 96.2	1,463.2 ± 99.5	n.s. (*t*-test)
3 Day 5	Open-field test	Total distance (cm)	2,622.2 ± 204.4	2,289.5 ± 2,234.0	n.s. (*t*-test)	3,978.3 ± 149.6	3,920.6 ± 262.2	n.s. (*t*-test)
		Total time in center area (sec)	7.7 ± 1.8	20.6 ± 12.8	n.s. (Wilcoxon)	14.0 ± 1.9	9.0 ± 1.7	n.s. (*t*-test)
4 Day 6	Light–dark box test	Time in light area (sec)	232.8 ± 30.8	184.2 ± 29.9	n.s. (*t*-test)	148.5 ± 23.7	171.6 ± 23.0	n.s. (*t*-test)
		No. of times of Transition	27.7 ± 4.5	27.9 ± 3.5	n.s. (*t*-test)	29.2 ± 4.1	31.9 ± 4.8	n.s. (*t*-test)
		Latency of transition (sec)	109.8 ± 29.1	55.2 ± 10.3	n.s. (Wilcoxon)	36.0 ± 11.9	46.0 ± 154.0	n.s. (Wilcoxon)
5 Day 7	Elevated plus maze test	Total distance (cm)	1,004.5 ± 54.7	854.7 ± 97.0	n.s. (*t*-test)	1,303.6 ± 66.1	1,399.2 ± 125.7	n.s. (*t*-test)
		Total time in open arm (sec)	7.7 ± 2.9	55.2 ± 47.7	n.s. (Wilcoxon)	30.8 ± 8.8	63.1 ± 20.4	n.s. (Wilcoxon)
		Open-arm entry/total entry (%)	19.5 ± 4.1	28.3 ± 5.6	n.s. (Wilcoxon)	22.2 ± 3.1	29.8 ± 4.3	n.s. (*t*-test)
6 Day 8	Resident–intruder test	No. of bites	1.6 ± 1.4	1.7 ± 1.0	n.s. (Wilcoxon)	4.8 ± 2.9	0.4 ± 0.3	n.s. (Wilcoxon)
		Latency of bites (sec)	782.1 ± 79.2	817.5 ± 47.2	n.s. (Wilcoxon)	726.0 ± 91.2	846.0 ± 36.9	n.s. (Wilcoxon)
7 Day 9	Rota-rod test	Time (sec)	42.2 ± 3.9	61.8 ± 12.6	n.s. (*t*-test)	36.9 ± 10.1	64.8 ± 11.7	n.s. (Wilcoxon)
8 Day 10	Startle response and prepulse inhibition test		See Fig. 1			See Fig. 1		
9 Day 11	Hotplate test	Time (sec)	25.6 ± 2.3	21.2 ± 1.8	n.s. (Wilcoxon)	20.5 ± 1.1	24.0 ± 1.5	$*p < 0.05$ (Wilcoxon)
10 Day 11	Tail-flick test	Time (sec)	2.5 ± 0.3	2.5 ± 0.2	n.s. (Wilcoxon)	2.1 ± 0.1	2.7 ± 0.3	n.s. (Wilcoxon)

*Statistical significance is indicated (n.s., not significant). Values are mean ± SEM. 1: Hesr1 wild-type (+/+), n = 16; Hesr1 KO (−/−), n = 20; Hesr2(+/+), n = 9; Hesr2(−/−), n = 15. 2: Hesr1(+/+), n = 18; Hesr1(−/−), n = 22; Hesr2(+/+), n = 12; Hesr2(−/−), n = 15. 3–10: Hesr1(+/+), n = 11; Hesr1(−/−), n = 12; Hesr2(+/+), n = 12; Hesr2(−/−), n = 15.

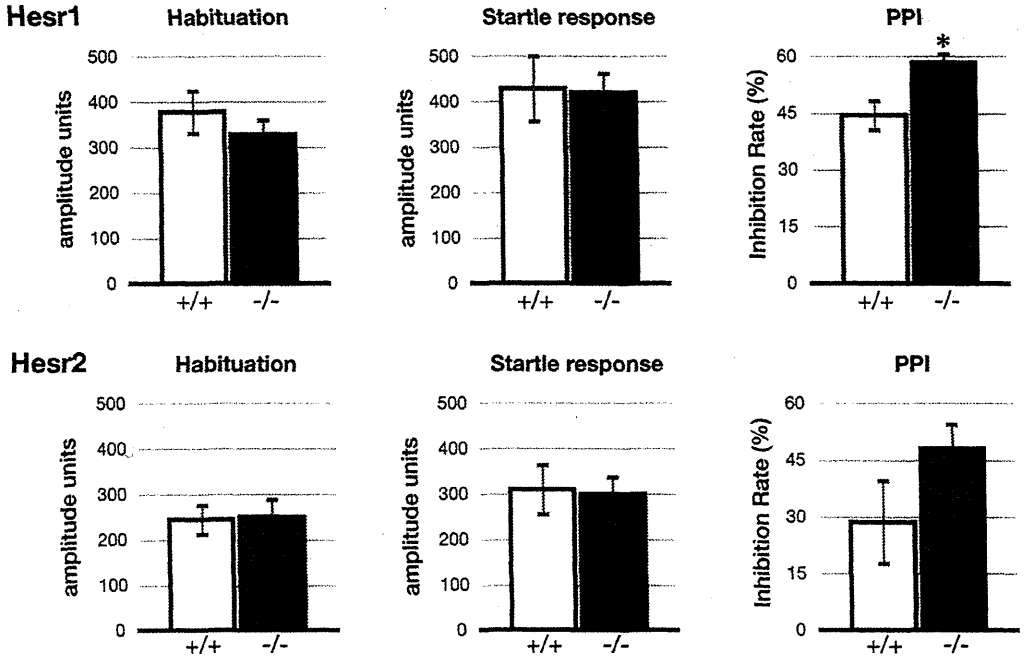

Fig. 1. Enhanced prepulse inhibition in Hesr1 KO mice. Values indicate means ± SEM. $*P < 0.05$, Student's *t*-test, wild-type (+/+) vs. knockout (KO; −/−) mice.

1968; Deacon, 2013). The apparatus consisted of a black striated rod (3-cm diameter) at a 20-cm height from the floor (Ohara Co. Ltd.). The animal was placed on the rod with constant low-speed rotation (5 rpm). After a few seconds, when the mouse had adjusted to walking on the rod, the test was started. In a trial, the rotation was gradually accelerated, from 5 to 40 rpm, over a 5-min period. The time at which the mouse fell off the rotating cylinder was measured automatically. Two trials were performed for each mouse, and the higher score was used for statistical analysis.

Startle Response and Prepulse Inhibition Test

Acoustic startle response (reflex) and its prepulse inhibition (PPI) were also measured. Startle response PPI is an operational measure of sensorimotor gating, deficits of which are observed in schizophrenia patients and related to the dopaminergic system (Geyer et al., 2001). Startle reactivity was measured using a startle chamber (San Diego Instruments, San Diego, CA). The chamber consisted of a clear resin cylinder resting on a platform inside a ventilated box. A high-frequency loudspeaker inside the chamber produced both a continuous background noise of 65 dB and various acoustic stimuli. Vibrations of the cylinder caused by the startle response of the animal were transduced into signals by a piezoelectric accelerometer beneath the cylinder that translated movement into changes in voltage (millivolts). These signals were then recorded by the computer system.

All PPI test sessions consisted of startle trials (pulse-only), prepulse trials (prepulse + pulse), and no-stimulus trials (nostim). In total, 38 trials, including habituation trials, were performed during one set of tests for each animal, and the average amplitude was used to determine the acoustic startle response. The pulse-alone trial consisted of a 40-msec, 120-dB pulse of broad-band noise. PPI was measured by prepulse trials that consisted of a 20-msec noise prepulse sound followed by a 30-msec, 120-dB sound pulse with a 70-msec interval. The acoustic prepulse intensities were 5, 10, and 15 dB above the 65-dB background noise (i.e., 70, 75, and 80 dB). The nostim trial consisted of background noise only. Each trial was presented six times in pseudorandom order with a variable interval (range 5–10 sec). The test session began and ended with four presentations of the pulse-only trial (as habituation trials described above). The average values of PPI under all prepulse conditions are presented in Figure 1. PPI rates were calculated using the following formula: inhibition rate = (1 − [prepulse + pulse]/[pulse-only]) × 100.

Hotplate Test

Pain sensation was evaluated in the hotplate test, which focuses on thermal sensitivity, as described previously (Koide et al., 2000). A hotplate surrounded by a wall made of acrylic acid resin (Muromachi Kikai Co., Ltd., Tokyo, Japan) was heated and maintained at 52°C during the test. Immediately following placement of mice on the plate, the time to lick the hind limb was measured by an observer.

Tail Flick Test

Sense of pain was assessed using the tail flick test as described previously (Koide et al., 2000). Mice were held gently with the tail placed on the apparatus (Muromachi Kikai

Co., Ltd.) to measure the latency of the tail flick response elicited by applying radiant heat to the ventral surface of the tail. Cutoff time for the heat stimulus was recorded automatically with an infrared sensor three times per individual at three different positions on the tail. The median value was used for statistical analysis.

Sample Preparation

Stereotactic coordinates (Franklin and Paxinos, 2008) were used to dissect out the forebrain region (+2 to −4.0 relative to bregma) and midbrain region, including the ventral tegmental area (VTA) and substantia nigra (SN; −3.00 to −4.00 to bregma). Tissues were collected after the last behavioral battery on that day. The midbrain was used for measurement of DAT and TH mRNA, and the forebrain was evaluated in terms of expression of D1 and D2 receptors. The forebrain region, which contains dopaminergic axon terminals, was also used for Western blotting for DAT and TH proteins. The right side of these regions was used for RT-PCR, and the left side was used for Western blotting.

Real-Time Quantitative PCR Analysis

Homogenization and total RNA extraction were conducted using Trizol (Invitrogen, Carlsbad, CA) according to the manufacturer's protocol. First-strand cDNA was synthesized using the PrimeScript RT-PCR System (TaKaRa, Shiga, Japan) according to the manufacturer's instructions. cDNA templates (50 ng) were used for real-time PCR. Real-time quantitative PCR was carried out using the comparative ΔGC method and the StepOne System (Applied Biosystems, Darmstadt, Germany). Each PCR product was synthesized using the SYBR Green reagent (Applied Biosystems) with the same oligonucleotide primers as were used in our previous report (Fuke et al., 2006). Average putative expression values from replicate PCRs were normalized to those of the GAPDH gene as an internal control. The ratios of the gene expression levels of the KO mice to those of the wild-type were then calculated.

Western Blotting

The collected brains were lysed in buffer containing 150 mM NaCl, 50 mM Tris-HCl (pH 7.4–7.6), 1 mM EDTA, 1% Triton X-100, and protease inhibitor cocktail (Sigma-Aldrich, St. Louis, MO) with a glass homogenizer and were left at 4°C for 30–60 min. Samples were centrifuged (13,000 rpm, 20 min, 4°C) to remove cellular debris. The protein concentration in the solubilized material was determined by DC protein assay (Bio-Rad, Hercules, CA). After addition of 4× protein sample buffer containing 0.25 M Tris-HCl (pH 6.8), 20% 2-mercaptoethanol, 8% sodium dodecyl sulfate (SDS), 20% sucrose, and 0.02% BPB, samples were incubated at 65°C for 15 min. Samples (30 μg/μl) were stored at −20°C until use.

Electrophoresis and Transfer

Samples (30 μg protein per lane) and the BenchMark Pre-Stained Protein Ladder (Invitrogen) were separated by SDS-PAGE and transferred to PVDF membranes (Immobilon-P; IPVH00010; Millipore, Bedford, MA). Membranes were equilibrated with methanol for 1 min, then MilliQ water for 2 min, and finally transfer buffer (195 mM glycine, 25 mM Tris, 20% methanol) for at least 30 min before transfer.

Antibodies

The primary antibodies rat anti-DAT (1:1,000; MAB369; Chemicon, Temecula, CA) and rabbit anti-actin (1:600; A2066; Sigma-Aldrich) were diluted in TBST containing 1% BSA; rabbit anti-TH (1:1,000; AB152; Chemicon) was diluted in TBST without BSA. For secondary antibodies, horseradish peroxidase (HRP)-linked anti-rabbit IgG (1:5,000; No. 7074; Cell Signaling, Beverly, MA) was diluted in TBST, and HRP-linked anti-rat IgG (1:5,000; No. 7077; Cell Signaling) was diluted in TBST containing 5% dry skim milk.

Immunoblotting

Membranes were first blocked for 1 hr in TBST buffer (50 mM Tris-HCl, pH 7.4–7.6, 150 mM NaCl, 0.1% Tween 20) containing 5% dry skim milk, then incubated with each primary antibody solution overnight at 4°C and with the HRP-conjugated secondary antibody solution for 1 hr at room temperature. Before and after incubation with each antibody, membranes were washed three times for 10 min with TBST. Protein bands were visualized using ECL prime for DAT and TH, or Luminata Forte (Millipore) for actin. Images of protein bands were captured by the LAS-3000 system (Fujifilm, Tokyo, Japan) and analyzed with the incorporated software (Multigauge ver. 2.3). Before incubation with the primary antibody, membranes were cut horizontally at about 50 kDa and divided into two pieces. The upper part was used for immunoblotting of DAT and the other for actin.

For immunoblotting of TH, membranes used for DAT were stripped by incubation with 0.2 M glycine solution (pH 2.8) for 30 min at room temperature. Before and after stripping, membranes were washed three times for 10 min with TBST. Next, blocking with TBST containing 5% skim milk was performed for 30 min. The process described above, except for the immunoreaction for TH, was then conducted.

Injection of a Dopamine Agonist Before PPI Measurement

PPI measurements were conducted as described above. Naïve mice were used for this test. Saline (vehicle) and the dopamine D1 and D2 receptor agonist apomorphine (apomorphine hydrochloride hemihydrate; A4393-100MG; Sigma-Aldrich) were injected intraperitoneally into the mice 15 min before each PPI measurement. The PPI tests were conducted three times every 5 days (4-day intervals among tests) with the same individuals. The doses were 1 or 5 mg/kg of apomorphine or saline (vehicle). An individual mouse received all three doses of injections in sequence before each test without repetition of the same dose. The order of the three injections (saline, 1 mg/kg, and 5 mg/kg) was randomized among the animals so that drug effects were counterbalanced. The average PPI values under all prepulse conditions are presented in Figure 4.

Statistical Analyses

Statistical analyses were performed in JMP 8.0 software (SAS Institute, Cary, NC). All values are reported as

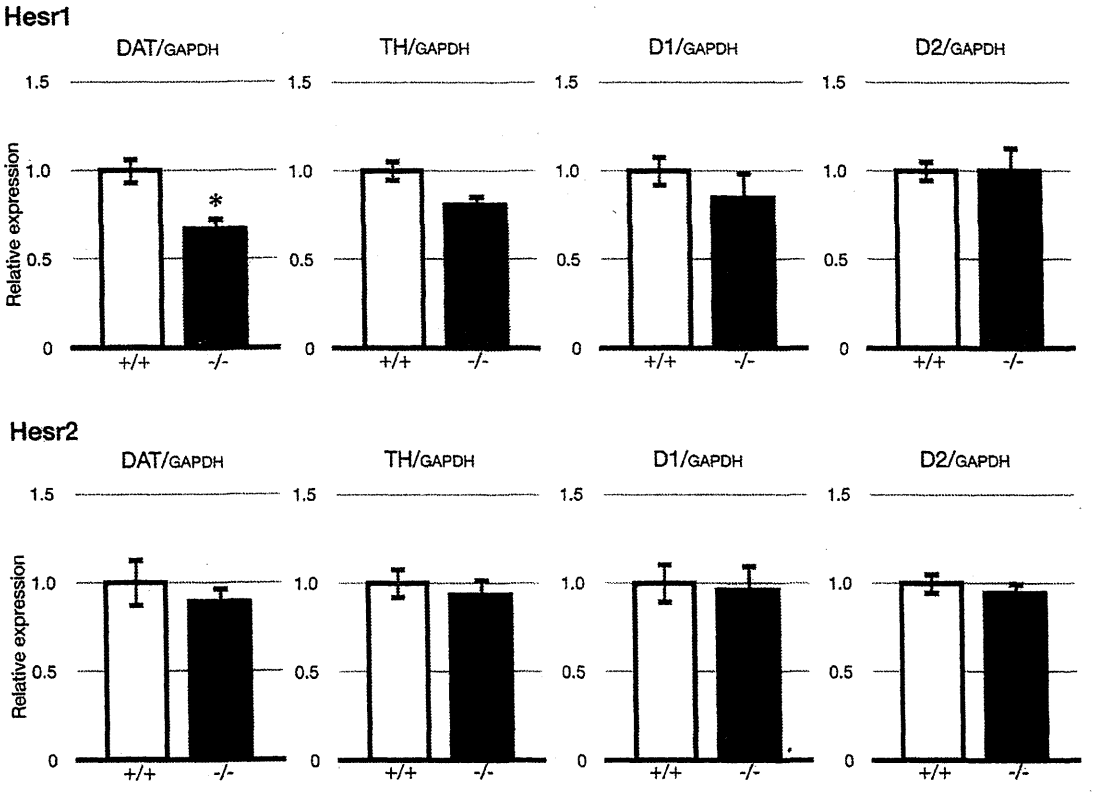

Fig. 2. Real-time quantitative PCR analysis of dopamine-related gene expression in the wild-type and knockout mice. Relative mRNA expressions of dopamine transporter (DAT), tyrosine hydroxylase (TH), dopamine D1 receptor (D1), and dopamine D2 receptor (D2) were standardized to the wild type (+/+) expression in each Hesr1 (upper panels) and Hesr2 (lower panels) knockout line. $*P < 0.05$, Student's *t*-test. The numbers of mice used were as follows: Hesr1(+/+), n = 5; Hesr1(−/−), n = 4; Hesr2(+/+), n = 5; Hesr2(−/−), n = 5.

mean ± SEM. Data of the Hesr1 and Hesr2 lines were analyzed separately in all statistical tests. Student's *t*-tests were used to detect statistically significant differences between two objects (Table I, Figs. 1–3) when the data were normally distributed. When the data were not normally distributed, the Wilcoxon test was applied (Table I, Fig. 1). The normality was confirmed by Shapiro-Wilk's W test. The *t*-test (for a between-subject factor: genotype) and Dunnett's method (for a within-subject factor: dose) were used as post hoc tests after the generalized linear model test had been performed (Fig. 4, Supp. Info. Figs. 1–4). Differences were considered to be statistically significant at $P < 0.05$.

RESULTS

Behavioral Test Battery

A summary of the behavioral results is shown in Table I. Among the 10 tests, a significant difference between wild-type and KO mice was detected in only the PPI test in the Hesr1 KO line. In the Hesr2 KO line, a significant difference was observed only in the hotplate test. For some tests, further temporal analysis was conducted (see Supp. Info. Figs. 1–4).

In the PPI test (Fig. 1), enhanced PPI was detected in the Hesr1 KO mice. The average value of PPI (Fig. 1) was significantly higher in the Hesr1 KO mice than in the wild-type mice. Values of the startle responses in the habituation and pulse-only trials were comparable (Fig. 1). In the Hesr2 group, there was no significant difference between genotypes in any index (habituation, startle response, or PPI in Fig. 1).

For the Hesr1 strain, the mean body weight of the wild type was 28.0 ± 0.9 g, whereas for KO mice it was 25.4 ± 0.9 kg. For the Hesr2 strain, the mean body weight of the wild type was 28.8 ± 0.5 g, whereas for KO mice it was 27.0 ± 0.5 kg. Thus, the body weights of both Hesr1 and Hesr2 KO mice were significantly lower than those of wild-type animals (Student's *t*-test, $P < 0.05$).

Expression of DAT, TH, and Dopamine Receptor D1 and D2 Receptors: Quantitative PCR Analysis

Expression levels of mRNA for DAT, TH, and D1 and D2 receptors were assessed by real-time PCR. As shown in Figure 2, the DAT expression level differed in the Hesr1 KO line, but no other significant difference was detected in either the Hesr1 or the Hesr2